Fine-scale application of WRF-CAM5 during a dust storm episode over East Asia: Sensitivity to grid resolutions and aerosol activation parameterizations

Kai Wang[a,*], Yang Zhang[a,e,**], Xin Zhang[a], Jiwen Fan[b], L. Ruby Leung[b], Bo Zheng[c], Qiang Zhang[d], Kebin He[c,e]

[a] Department of Marine, Earth, and Atmospheric Sciences, NCSU, Raleigh, NC, USA
[b] Atmospheric Sciences and Global Change Division, Pacific Northwest National Laboratory, Richland, WA, USA
[c] State Key Joint Laboratory of Environment Simulation and Pollution Control, School of Environment, Tsinghua University, Beijing, China
[d] Ministry of Education Key Laboratory for Earth System Modeling, Center for Earth System Science, Tsinghua University, Beijing, China
[e] Collaborative Innovation Center for Regional Environmental Quality, Beijing, China

ARTICLE INFO

ABSTRACT

An advanced online-coupled meteorology and chemistry model WRF-CAM5 has been applied to East Asia using triple-nested domains at different grid resolutions (i.e., 36-, 12-, and 4-km) to simulate a severe dust storm period in spring 2010. Analyses are performed to evaluate the model performance and investigate model sensitivity to different horizontal grid sizes and aerosol activation parameterizations and to examine aerosol-cloud interactions and their impacts on the air quality. A comprehensive model evaluation of the baseline simulations using the default Abdul-Razzak and Ghan (AG) aerosol activation scheme shows that the model can well predict major meteorological variables such as 2-m temperature (T2), water vapor mixing ratio (Q2), 10-m wind speed (WS10) and wind direction (WD10), and shortwave and longwave radiation across different resolutions with domain-average normalized mean biases typically within ± 15%. The baseline simulations also show moderate biases for precipitation and moderate-to-large underpredictions for other major variables associated with aerosol-cloud interactions such as cloud droplet number concentration (CDNC), cloud optical thickness (COT), and cloud liquid water path (LWP) due to uncertainties or limitations in the aerosol-cloud treatments. The model performance is sensitive to grid resolutions, especially for surface meteorological variables such as T2, Q2, WS10, and WD10, with the performance generally improving at finer grid resolutions for those variables. Comparison of the sensitivity simulations with an alternative (i.e., the Fountoukis and Nenes (FN) series scheme) and the default (i.e., AG scheme) aerosol activation scheme shows that the former predicts larger values for cloud variables such as CDNC and COT across all grid resolutions and improves the overall domain-average model performance for many cloud/radiation variables and precipitation. Sensitivity simulations using the FN series scheme also have large impacts on radiations, T2, precipitation, and air quality (e.g., decreasing O_3) through complex aerosol-radiation-cloud-chemistry feedbacks. The inclusion of adsorptive activation of dust particles in the FN series scheme has similar impacts on the meteorology and air quality but to lesser extent as compared to differences between the FN series and AG schemes. Compared to the overall differences between the FN series and AG schemes, impacts of adsorptive activation of dust particles can contribute significantly to the increase of total CDNC (~45%) during dust storm events and indicate their importance in modulating regional climate over East Asia.

1. Introduction

Aerosols play complicated and important roles in global and regional climate by directly changing the earth radiation balance through scattering or absorbing of solar radiation or indirectly affecting cloud formation, lifetime, and properties through activation as cloud condensation nuclei (CCN) or ice nuclei (IN) (Yu, 2000; Yu et al., 2014). Among the major processes associated with aerosol particles, aerosol-cloud interactions have been widely recognized as the most important and uncertain aspect of climate changes (Boucher et al., 2013). To better understand and assess the impacts of aerosols on climate, it is essential to examine major processes such as aerosol activation (also

known as cloud droplet nucleation) that are critical to aerosol-cloud interactions. Aerosol activation affects not only cloud droplet number concentration (CDNC) but also other cloud properties such as cloud liquid water content and cloud optical thickness (COT).

Due to the lack of a complete aerosol activation theory, aerosol activation has been parameterized in all climate models (Abdul-Razzak and Ghan, 2000). Many physically-based aerosol activation parameterizations that account for aerosol size distribution, chemical composition, and ambient atmospheric conditions have been developed in the past (Abdul-Razzak and Ghan, 2000; Cohard et al., 2000; Nenes and Seinfeld, 2003; Fountoukis and Nenes, 2005; Ming et al., 2006). Among them, two parameterizations are most commonly used including those developed by Abdul-Razzak and Ghan (2000) (hereafter referred to as AG00) and Fountoukis and Nenes (2005) (hereafter referred to as the base FN05) based on the Köhler theory (Köhler, 1936). AG00 uses a semi-empirical formula to calculate the supersaturation and has been widely used in many global and regional models (Ghan et al., 2012). The base FN05 scheme explicitly calculates supersaturation through numerical iterations. A recent study by Ghan et al. (2011) found that FN05 can predict more consistent activation fraction of aerosols than the AG00 scheme when compared to numerical solutions. Several updates have been added to the base FN05 recently, which include the effect of convective entrainment on aerosol activation (Barahona and Nenes, 2007) (hereafter referred to as BN07), the adsorptive activation pathway for insoluble particles such as dust (Kumar et al., 2009) (hereafter referred to as K09), and the treatment of kinetic limitations of giant CCN (Barahona et al., 2010) (hereafter referred to as B10). The base FN05 scheme with the aforementioned updates of BN07, K09, and B10 (hereafter referred to as FN series) has been recently implemented into both global (Gantt et al., 2014) and regional models (Zhang, 2014; Zhang et al., 2015a). Compared to AG00, FN series is found to generally better predict variables representing aerosol-cloud interactions such as CDNC, cloud liquid water path (LWP), and COT.

In the past two decades, East Asia, especially China, has experienced rapid economic and population growth and fast industrialization and urbanization (Wang et al., 2010). Hence this region has emerged as one of the largest contributors to global climate change (Boucher et al., 2013). Large amounts of anthropogenic and natural emissions of aerosols (especially dust) from East Asia resulted in extremely high aerosol concentrations and significantly degraded the regional air quality locally and downwind (e.g., North America) through long-range transport (Heald et al., 2006; Wang et al., 2009, 2012). In addition to high aerosol concentrations, East Asia encompasses regions with complex topography and distinct weather system that may further complicate the interactions of air quality and regional climate (Akimoto, 2003). During springtime, strong mid-latitude cyclones that pass through western China may lift dust particles from the surface of Taklimakan Desert and Gobi Desert to high altitude (Chen et al., 2013), which allows them to be transported to northern and eastern China (Bian et al., 2011) where anthropogenic aerosol concentrations are very high. During the transport, dust particles become aging and mix with other soluble secondary aerosols and can act as efficient CCN and IN (Kumar et al., 2009). Therefore, dust particles from dust storm events may have large influences on aerosol-cloud interactions in East Asia. In spring 2010, due to the worst drought in the century over western and southwestern China, several dust storm events have been reported (Bian et al., 2011; Li et al., 2011; Zhao et al., 2011), which provide ideal testbeds for studying the impacts of dust on aerosol-cloud interactions and air quality.

It has been reported in the past that the skill of climate/air quality models in simulating meteorology and air quality can be highly dependent on grid resolutions especially over areas with high pollutants and/or with complex terrains (Fountoukis et al., 2013; Zhang et al., 2013; Kuik et al., 2016). For example, Fountoukis et al. (2013) reported that the use of high grid resolution can decrease model biases for

certain aerosol species such as black carbon (BC). Kuik et al. (2016) found that by using the Weather Research and Forecasting model coupled with chemistry (WRF/Chem), the model performance was improved from 15-km to 3-km resolution for major meteorological and chemical variables, but this is not the case from 3-km to 1-km resolution. Very few studies have examined aerosol-cloud interactions using fine grid resolutions (e.g., 4-km) and complex aerosol activation mechanisms over highly polluted areas such as East Asia. Such studies will provide valuable information to guide future modeling studies for East Asia.

To improve our understanding of aerosol-cloud interactions under extreme high aerosol conditions, we apply the regional air quality/climate model, the WRF model coupled with the physics package of Community Atmospheric Model version 5 (WRF-CAM5) (Ma et al., 2013; Lim et al., 2014; Chen et al., 2015; Zhang et al., 2015a,b) in spring 2010 to investigate the impacts of high aerosol concentrations, different horizontal grid resolutions, and different aerosol activation parameterizations on aerosol-cloud interactions over East Asia. The objectives of this study are to (1) perform a comprehensive model evaluation of WRF-CAM5 at different grid resolutions by conducting triple-nested simulations at 36-, 12-, and 4-km grid resolutions; (2) investigate the impacts of two aerosol activation schemes (i.e., AG00 and FN series) on simulating aerosol-cloud interactions and regional air quality through feedbacks across different grid resolutions and the contribution of dust particles to aerosol-cloud interactions through the adsorptive activation mechanism (i.e., K09).

2. Model description, simulation setup, and evaluation protocols

2.1. Model description

The WRFv3.4-CAM5 model initially developed at the Pacific Northwest National Laboratory (PNNL) (Ma et al., 2013) incorporated the physical and aerosol packages of the global model CAM5 into the WRF/Chem model (Grell et al., 2005). Compared to other online-coupled models, this model is designed to investigate atmospheric processes in a multi-scale framework and provide a regional modeling framework for evaluating physics and aerosol parameterizations used in global climate models (Ma et al., 2013). The WRF-CAM5 model includes state-of-science cloud schemes such as the Morrison two-moment cloud microphysics scheme (Morrison and Gettelman, 2008), and the Zhang-MacFarlane (ZM) convective cloud scheme (Zhang and McFarlane, 1995) with explicit aerosol-convective cloud feedbacks (Song and Zhang, 2011) implemented and evaluated by Lim et al. (2014), and an up-to-date ice-nucleation parameterization for mixed-phase and ice clouds (Niemand et al., 2012). The 3-mode Modal Aerosol Module (MAM3) (Liu et al., 2012) has been fully implemented and tested in this version of WRF-CAM5. MAM3 includes three modes: Aitken, accumulation, and coarse modes, with different internally-mixed aerosol components such as sulfate (SO_4^{2-}), primary organic aerosols (POA), secondary organic aerosols (SOA), BC, dust, and sea-salt. Ammonium (NH_4^+) is implicitly simulated and assumed to co-exist with SO_4^{2-} as ammonium bisulfate (NH_4HSO_4). Nitrate (NO_3^-) is not simulated in MAM3 which may introduce uncertainties in simulating aerosols. There is a simplified SOA scheme in WRF-CAM5 in which five volatile organic compounds (VOCs) can generate SOA with fixed mass yields (i.e., 5% for big alkanes, 5% for big alkenes, 15% for toluene, 4% for isoprene, and 25% for monoterpenes).

The original WRF-CAM5 model is further developed recently at North Carolina State University through implementation of an alternative aerosol activation parameterization (i.e., the FN series) (Zhang, 2014; Zhang et al., 2015a). Major differences between AG00 and the base FN05 include 1) different approaches to calculate the maximum supersaturation; 2) different values of condensation coefficient (i.e., 1.0 in AG00 vs 0.06 in FN05); 3) absence (AG00) or inclusion (FN05) of gas kinetic effect on aerosol activation; and 4) different dependency of
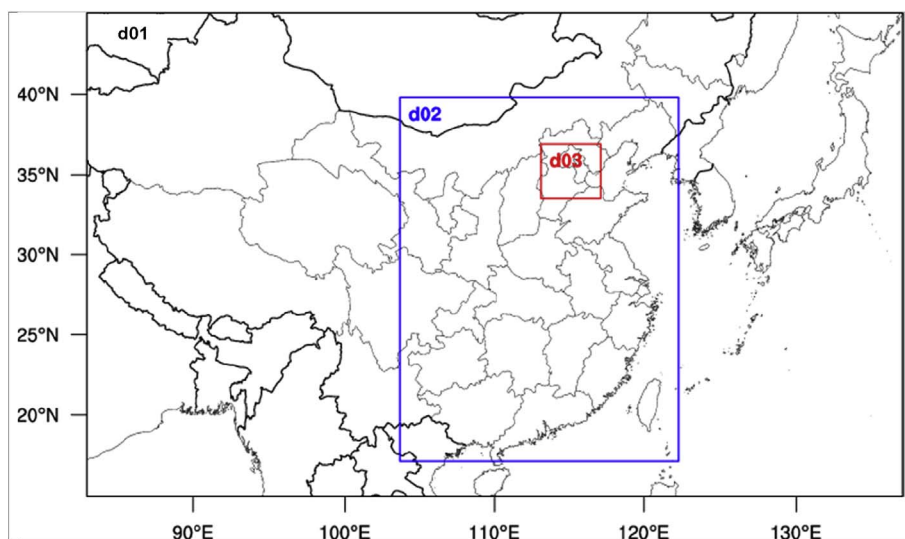
Fig. 1. Simulation domains: D01 (black) over East Asia, D02 (blue) over eastern China, and D03 (red) over Beijing and its surrounding areas. (For interpretation of the references to colour in this figure legend, the reader is referred to the Web version of this article.)

surface tension and Kelvin effect on temperature. More details of those differences can be found in Zhang (2014) and Zhang et al. (2015a). In addition, the subsequent updates of FN05 may further affect the differences between FN05 series and AG00. For example, K09 considers aerosol adsorptive activation from insoluble aerosols (e.g., dust and BC), which may further increase the fraction of activated aerosols so the impacts will be examined in this study.

2.2. Simulation configurations and setup

The WRF-CAM5 model with the addition of the FN series parameterizations as described in Section 2.1 is applied to a nested East Asia domain during a dust storm episode in spring (i.e., March to May) 2010. The triple-nested domain includes three subdomains with horizontal resolutions of 36-, 12-, and 4-km, respectively, and vertical resolution of 23 layers (from surface to 100 hPa and approximately 8 layers within the PBL). As shown in Fig. 1, the level-1 domain (D01) covers the whole East Asia including China, Japan, North and South Korea, Mongolia, India, and other southeastern Asian countries. The level-2 domain (D02) covers eastern and southeastern China. The level-3 domain (D03) covers the capital city of China, Beijing, and its surrounding areas. The simulations use one-way nesting to achieve higher spatial resolution. Details of the model components and configurations are summarized in Table 1. The meteorological initial/boundary conditions (ICONs/BCONs) are generated from the National Center for Environmental Predictions Final Analysis (NCEP-FNL) and the chemical ICONs/BCONs are adapted from simulations of the Community Multiscale Air Quality (CMAQ) modeling system. Offline anthropogenic emissions for mainland China are from the Multi-resolution Emission Inventory for China (MEIC; http://www.meicmodel.org/) and those for the rest of the domain are from the Intercontinental Chemical Transport Experiment (INTEX-B) inventory (Zhang et al., 2009). Biogenic emissions are calculated online through the Model of Emissions of Gases and Aerosols from Nature (MEGAN) version 2. Dust and sea-salt emissions are also generated online using the module developed by Zender et al. (2003) and implemented by Wang et al. (2012) for dust and Gong et al. (2002) for sea-salt, respectively. A one month (i.e., February 2010) spin-up is performed to minimize the impacts of chemical ICONs. The meteorological fields are also re-initialized every five days to construct an acceptable meteorological field for the chemistry simulations while allowing for sufficient time for chemistry-meteorology feedbacks.

Three sets of simulations are conducted to achieve the objectives of this work. These include the baseline simulation (hereafter referred to as BASE) using the WRF-CAM5 with the default AG00 aerosol activation parameterization. The first sensitivity simulation (hereafter

referred to as SEN1) includes the same treatments as BASE except for replacing the aerosol activation parameterization with the FN series. The second sensitivity simulation (hereafter referred to as SEN2) is similar to SEN1 but the ability of dust particles to serve as CCN is turned off (i.e., The FN series without K09). All three simulations are performed over the triple-nested domains. These simulations are designed to evaluate the capability of WRF-CAM5 in simulating the regional meteorology, air quality, and their feedbacks as well as the sensitivity of the model predictions to different horizontal grid resolutions and aerosol activation treatments. Comparison between SEN1 and BASE is used to assess the potential for model improvement in representing aerosol-cloud interactions by using a more advanced aerosol activation parameterization based on the FN series. Differences between SEN1 and SEN2 are used to evaluate the contribution of dust particles to aerosol-cloud interactions especially during dust storm events.

2.3. Observational data and evaluation protocols

A comprehensive model evaluation is conducted using available meteorological and chemical data from various surface networks, radiosonde database, satellite retrievals, and reanalysis data. Variables evaluated in this work include surface meteorological variables such as 2-m temperature (T2), water vapor mixing ratio (Q2), 10-m wind speed (WS10) and direction (WD10), and precipitation; surface chemical variables such as carbon monoxide (CO), nitrogen monoxide (NO), nitrogen dioxide (NO_2), sulfur dioxide (SO_2), ozone (O_3), particulate matter with aerodynamic diameter less or equal to 10 μm (PM_{10}) derived based on the Air Pollution Index (API), particulate matter with aerodynamic diameter less or equal to 2.5 μm ($PM_{2.5}$) and its components and suspended particulate matter (SPM; approximated as PM_{10}), column chemical variables such as CO column, NO_2 column, SO_2 column, and tropospheric ozone residual (TOR), and radiation/cloud variables such as aerosol optical depth (AOD), downward shortwave and longwave radiation (SWDOWN and LWDOWN), shortwave and longwave cloud radiative forcing (SWCF and LWCF), outgoing longwave radiation (OLR), COT, cloud fraction (CF), CCN, and precipitable water vapor (PWV), CDNC, LWP, and ice water path (IWP). More details on the datasets, variables, data frequencies, and data sources can be found in Tables S1–S2 in the supplementary material.

Model evaluation is performed following the protocol proposed by Zhang et al. (2006, 2012a, b) including metrics such as monthly spatial distribution, hourly or daily temporal variation at selected sites, and domain-average statistics. The performance statistics for individual variables are calculated separately for different networks or datasets due to inherent differences in observational method, data collection,

Table 1
The model configurations of the WRF-CAM5 simulations.

Attributes	Model Configurations
Simulation period	March to May 2010
Domain	East Asia
Horizontal resolution	36-km, 12-km, 4-km (one-way nested)
Vertical resolution	23 layers from surface to 100 mb
Physical options	
Shortwave radiation	Rapid and accurate Radiative Transfer Model for GCM (RRTMG)
Longwave radiation	RRTMG (Clough et al., 2005)
PBL	University of Washington (Bretherton and Park, 2009)
Land surface	the National Center for Environmental Prediction, Oregon State University, Air Force, and Hydrologic Research Lab (NOAH) (Chen and Dudhia, 2001)
Microphysics	Morrison two-moment (Morrison and Gettelman, 2008)
Cumulus	Zhang and McFarlane (1995) with update of Song and Zhang (2011)
Aerosol activation	AG00 (Abdul-Razzak and Ghan, 2000) and FN05 (Fountoukis and Nenes, 2005) with updates of Barahona and Nenes (2007), Kumar et al. (2009), Barahona et al. (2010)
Ice nucleation	Niemand et al. (2012)
Chemical options	
Gas-phase chemistry	Carbon Bond Mechanism version Z (CBM-Z) (Zaveri and Peters, 1999))
Aerosol module	CAM-MAM3 (Liu et al., 2012)
Photolysis	Fast Troposphere Ultraviolet Visible (F-TUV) (Tie et al., 2003)
Aqueous-phase chemistry	CAM simplified aqueous-phase chemistry (Barth et al., 2000)
Meteorological ICONs and BCONs	National Center for Environmental Prediction Final Analysis (NCEP-FNL)
Chemical ICONs and BCONs	CMAQ
Anthropogenic emission	MEIC and INTEX-B
Biogenic emission	Model of Emissions of Gases and Aerosols from Nature (MEGAN) version 2 (Guenther et al., 2006)
Dust emission	Wang et al. (2012) based on Zender et al. (2003)
Sea-salt emission	Gong et al. (2002)

and processing among different datasets. The statistical measures include the mean bias (MB), normalized mean bias (NMB), normalized mean error (NME), and correlation coefficient (R).

3. Comprehensive model evaluation of baseline simulation at various grid resolutions

3.1. Meteorological variables

Tables 2–4 summarizes the domain-average statistics for T2, Q2, WS10, WD10, and daily precipitation for BASE in the different domains. BASE predicts small cold biases for T2 throughout all domains, which are consistent with other modeling studies using either the fifth-generation Penn State/NCAR Mesoscale Model (MM5) or WRF (Zhang et al., 2011; Wang et al., 2012; García-Díez et al., 2013). BASE also predicts Q2 well with biases generally within $\pm 1 \, \mathrm{g \, kg^{-1}}$ over the different domains. A key improvement of this study compared to many previous WRF or WRF/Chem applications (e.g., Zhang et al., 2006, 2010; Tuccella et al., 2012) is the reduction of WS10 biases due to the utilization of a simple drag parameterization proposed by Mass and Ovens (2010), which helps to improve the model representation of low and moderate wind speeds by improving the representation of surface drag exerted by unresolved topography. As shown, the NMBs for WS10 is typically < 15% over different domains in this work while other studies using the WRF model typically predicted WS10 with ≥50% biases. Despite this improvement, there still exists large overprediction for high wind speed especially over the dust source regions (results not shown) such as Taklimakan Desert and Gobi Desert, which may lead to overprediction of dust emissions and further result in overprediction of dust/PM_{10} concentrations. The performance for precipitation is worse than other meteorological variables with generally wet biases especially in D01. The reasons might be complicated and some possible reasons are discussed below. First, a recent study by McMillen and Steenburgh (2015) found that the Morrison microphysics scheme tends to overpredict rainfall amount compared to other microphysics schemes in WRF, due to the high amount of predicted graupel and inclusion of cloud liquid water in the precipitation amount. Second, the NOAH land surface model used in this work is recently reported by Pei et al. (2014)

to potentially cause some positive biases for precipitation compared to other land surface models, due to the overestimation of surface evapotranspiration. Third, the lack of treatment of cloud-radiation feedbacks for convective cloud as recently reported by Alapaty et al. (2012) may also partially contribute to the wet biases.

The model sensitivity to grid resolutions for T2, Q2, WS10, WD10, and precipitation are further examined in Fig. 2 and Tables 3 and 4. To allow for a fair performance comparison across different resolutions (e.g., 36-km vs. 12-km or 12-km vs. 4-km), the 36-km simulation from D01 is compared with the 12-km simulation in the common region in D02. Similarly, the 36-km and 12-km simulations from D01 and D02, respectively, are compared with the 4-km results in the common region in D03. As shown in Fig. 2, in D02, T2 and precipitation are overall underpredicted at both 36-km and 12-km grid resolutions and Q2 and WS10 are overall overpredicted at both resolutions. The overpredictions of Q2 and WS10 are more dominated by sites with high moisture and low wind speed, respectively. The underpredictions of precipitation at both grid resolutions are dominated by sites with high precipitation. In D03, T2, Q2, and precipitation are generally underpredicted while WS10 is overpredicted at all grid resolutions. Despite the general consistent performance across different grid resolutions, more data pairs (i.e., sites) from the 36-km simulation (or the 12-km simulation) deviate from the 1:1 ratio line than the 12-km simulation (or the 4-km simulation) for all variables, indicating a better performance at the finer grid resolutions. The temporal performance for the above meteorological variables across different grid resolutions at representative sites is also examined in the supplementary materials. The results (as shown in Fig. S1 and Fig. 4) also generally indicate better performance for finer grid resolutions. Tables 3 and 4 also show improved performance for all major statistical metrics including MB, NMB, NME, and R for T2, Q2, WS10, and WD10, which is consistent with Fig. 2 and Fig. S1-S4. The above comparisons using scatter/temporal plots and domain-average statistics across different resolutions indicate improvements using finer resolutions and promises for fine scale resolution application of WRF-CAM5 in the future.

Fig. 3 shows the comparison of simulated seasonal mean vertical profiles of temperature, dew point temperature, wind speed, and wind direction against the sounding observations at four selected sites (i.e.,

Table 2
Performance statistics of BASE for spring (March–May) 2010 over domain D01.

Variables	Datasets	Mean Obs	Mean Sim	R	MB	NMB (%)	NME (%)
T2 (°C)	NCDC	12.8	11.4	0.96	−1.37	−10.7	16.6
Q2 (g kg^{-1})	NCDC	6.52	6.64	0.97	0.12	1.9	10.7
WS10 (m s^{-1})	NCDC	3.3	3.7	0.46	0.40	12.1	31.6
WD10 (degree)	NCDC	204.1	190.1	0.41	−14.0	−6.9	15.7
Precipitation (mm day^{-1})	NCDC	2.8	3.3	0.50	0.53	18.8	69.3
	GPCP	2.1	3.0	0.34	0.85	39.9	92.1
	TMPA	2.8	3.0	0.50	0.17	5.9	50.1
SWDOWN (W m^{-2})	CERES	211.3	239.9	0.89	28.6	13.5	14.5
LWDOWN (W m^{-2})	CERES	319.1	311.2	0.99	−7.9	−2.5	3.2
SWCF (W m^{-2})	CERES	−65.6	−49.8	0.89	−15.8	−24.2	27.1
LWCF (W m^{-2})	CERES	33.5	21.9	0.73	−11.6	−34.6	36.7
OLR (W m^{-2})	CDC	226.8	233.6	0.93	6.8	3.0	4.3
AOD	MODIS	0.40	0.25	0.33	−0.15	−37.3	53.6
	AERONET	0.54	0.37	0.32	−0.18	−32.4	60.9
COT	MODIS	15.4	9.9	0.78	−5.5	−35.8	50.6
CF	MODIS	0.66	0.59	0.65	−0.07	−10.6	20.3
CCN (10^9 cm^{-2})	MODIS	0.81	0.63	0.56	−0.17	−21.6	48.7
CDNC (cm^{-3})	MODIS	160.2	128.3	0.51	−31.9	−19.9	43.1
LWP (g m-2)	MODIS	98.0	51.4	0.72	−46.5	−47.5	58.4
IWP (g m-2)	MODIS	212.0	12.8	0.22	−199.2	−94.0	94.0
PWV (cm)	MODIS	1.75	1.88	0.98	0.13	7.7	14.6
PM$_{10}$ (µg m^{-3})	China	90.3	117.9	0.12	27.6	30.6	76.0
	Hong Kong	56.1	43.0	0.12	−13.1	−23.3	62.3
	Taiwan	69.6	29.7	0.41	−39.9	−57.4	58.1
	Japan	18.7	24.1	0.21	5.4	29.0	47.5
	South Korea	55.6	44.5	0.18	−11.1	−20.0	26.9
PM$_{2.5}$ (µg m^{-3})	Hong Kong	29.9	38.7	0.27	8.9	29.6	75.2
	Taiwan	34.2	21.8	0.44	−12.4	−36.2	38.6
CO (ppb for Hong Kong and ppm for others)	Hong Kong	886.6	521.0	0.37	−365.6	−41.2	44.5
	Taiwan	0.47	0.26	0.17	−0.21	−44.5	44.7
	Japan	0.40	0.18	0.07	−0.22	−54.5	55.1
	South Korea	0.45	0.23	0.26	−0.22	−48.8	48.9
Column CO (10^{18} molecules cm^{-3})	MOPITT	2.38	2.03	0.83	−0.35	−14.8	18.9
NO$_x$ (ppb)	Hong Kong	151.1	73.0	0.38	−78.1	−51.7	57.2
NO (ppb)	Japan	3.48	1.31	0.03	−2.17	−62.3	85.6
	Taiwan	4.58	2.95	0.07	−1.62	−35.5	68.9
NO$_2$ (ppb)	Hong Kong	66.4	56.2	0.38	−10.1	−15.2	42.3
	Taiwan	16.1	17.2	0.15	1.1	6.6	42.7
	Japan	9.4	7.8	0.02	−1.6	−17.0	63.2
	South Korea	15.5	15.7	0.16	0.21	1.3	50.6
Column NO$_2$ (10^{14} molecules cm^{-3})	SCIAMACHY	2.7	6.4	0.77	3.7	137.0	150.4
O$_3$ (ppb)	Hong Kong	40.5	45.2	0.56	4.6	11.5	67.9
	Taiwan	33.5	33.3	0.15	−0.14	−0.4	21.0
	Japan	43.9	36.0	0.30	−7.9	−18.1	19.9
	South Korea	34.9	30.7	0.31	−4.1	−11.9	30.3
TOR (DU)	OMI/MLS	31.3	37.0	0.68	5.7	18.2	21.5
SO$_2$ (ppb)	Hong Kong	11.1	32.8	0.30	21.6	194.1	209.2
	Taiwan	4.04	1.15	0.34	−2.9	−71.5	74.5
	Japan	2.2	1.1	0.16	−1.1	−49.6	71.5
	South Korea	4.3	3.0	0.37	−1.3	−31.0	46.3
Column SO$_2$ (DU)	SCIAMACHY	0.38	0.24	0.35	−0.14	−36.0	69.5

Beijing in D03 and Yanan, Hong Kong, and Taibei in D02). Before the comparison, significant tests (i.e., t-tests) using simulation and observational data for different variables over different sites have been conducted. The results show p-values from those tests are all < 0.005, indicating good confidence and statistical significance for the comparison. As shown in Fig. 3, BASE performs very well for the vertical profiles of temperature at all four sites at 12-km or 4-km grid resolutions. It also reproduces the vertical profiles of dew point temperature well below 300 hPa over Yanan and Taibei and below 700 hPa over Hong Kong. Large overprediction occurs below 250 hPa over Beijing and above 500 hPa over Hong Kong and large underprediction of dew point temperature occurs above 200 hPa over Beijing and Yanan, which indicate the model's inability in capturing moisture especially aloft. The overprediction of dew point temperature (i.e., atmospheric moisture), especially from lower to middle altitude in the atmosphere such as Beijing, may help explain the general overprediction of precipitation during the whole simulation period at individual sites such as Beijing as shown in Fig. S4. The model is also able to capture the prevailing wind in terms of both direction (mostly westerly wind) and speed (especially when wind speed is greater than 50 knots) above 500 hPa at all four sites. There are larger discrepancies between simulations and observations at lower altitude, especially over Beijing and Yanan, where the model fails to capture the observed southerly and southwesterly winds at the surface. The model discrepancies for wind direction in the lower altitude could be caused by complex surface topography and also biases associated with the simulated pressure gradient as reported by Jiménez et al. (2013).

3.2. Chemical variables

Fig. 4a shows the spatial distribution of seasonal mean PM$_{10}$ concentrations predicted by BASE in D01 overlaid with observations derived from the API data of China. PM$_{10}$ is used in this work to represent dust due to the lack of direct dust measurements. Extremely high PM$_{10}$ concentrations (> 250 µg m^{-3} in seasonal mean) are predicted by BASE over major dust source regions such as the Taklimakan Desert and Gobi

Table 3
Performance statistics of BASE for spring (March–May) 2010 over domain D02 (simulations over D01 and D02 against observations over D02).

Variables[a]	Datasets	Mean Obs	Mean Sim		R		MB		NMB (%)		NME (%)	
			D01	D02	D01	D02	D01	D02	D01	D02	D01	D02
T2	NCDC	14.2	13.8	13.8	0.97	0.97	−0.48	−0.43	−3.4	−3.0	10.5	8.9
Q2	NCDC	7.83	7.98	7.89	0.98	0.98	0.15	0.06	1.9	0.7	9.7	8.5
WS10	NCDC	3.2	3.4	3.4	0.46	0.55	0.21	0.17	6.4	5.4	28.2	26.4
WD10	NCDC	191.5	169.1	170.1	0.40	0.41	−22.4	−21.4	−11.7	−11.2	17.6	16.8
Precipitation	NCDC	3.44	2.99	3.07	0.67	0.72	−0.45	−0.37	−13.2	−10.8	49.1	45.4
	GPCP	1.9	3.0	3.1	0.58	0.62	1.1	1.3	58.5	69.0	91.8	96.6
	TMPA	3.4	3.1	3.0	0.77	0.75	−0.3	−0.4	−7.3	−13.0	35.8	38.6
SWDOWN	CERES	176.9	206.1	208.4	0.88	0.88	29.2	31.5	16.5	17.8	16.8	18.1
LWDOWN	CERES	331.0	326.1	324.9	0.99	0.99	−4.9	−6.1	−1.5	−1.9	2.1	2.4
SWCF	CERES	−83.9	−65.8	−64.0	0.90	0.90	−18.0	−19.8	−21.5	−23.6	23.1	24.8
LWCF	CERES	36.2	24.6	24.2	0.75	0.73	−11.6	−12.1	−32.1	−33.3	32.8	34.0
OLR	CDC	224.7	231.8	232.4	0.91	0.91	7.1	7.7	3.1	3.4	3.7	4.0
AOD	MODIS	0.52	0.42	0.41	0.18	0.19	−0.10	−0.11	−20.0	−20.8	47.9	47.4
	AERONET	0.56	0.37	0.37	0.33	0.33	−0.19	−0.19	−34.0	−33.0	62.3	60.8
COT	MODIS	19.5	17.6	16.9	0.81	0.81	−1.9	−2.6	−9.7	−13.4	40.5	38.3
CF	MODIS	0.74	0.64	0.64	0.62	0.63	−0.10	−0.10	−13.3	−13.4	17.4	17.2
CCN	MODIS	1.74	0.85	0.93	0.61	0.61	−0.89	−0.81	−50.9	−46.5	52.0	48.4
CDNC	MODIS	201.7	191.4	187.5	0.37	0.32	−10.3	−14.2	−5.1	−7.0	32.7	35.4
LWP	MODIS	122.5	98.2	93.5	0.73	0.74	−24.3	−29.0	−19.8	−23.7	43.5	41.3
IWP	MODIS	247.2	14.8	15.2	0.05	0.06	−232.4	−232.0	−94.0	−93.9	94.0	93.9
PWV	MODIS	1.89	2.17	2.16	0.98	0.98	0.28	0.27	14.9	14.1	16.5	16.0
PM$_{10}$	China	90.9	128.5	123.6	0.05	0.04	37.6	32.7	41.4	36.0	79.2	74.4
	Hong Kong	56.1	43.0	30.6	0.12	0.15	−13.1	−25.5	−23.3	−45.5	62.3	59.9
	Taiwan	69.6	29.7	35.8	0.41	0.60	−39.9	−33.7	−57.4	−48.5	58.1	49.4
PM$_{2.5}$	Hong Kong	29.9	38.7	26.2	0.27	0.33	8.9	−3.7	29.6	−12.3	75.2	54.7
	Taiwan	34.2	21.8	28.1	0.44	0.59	−12.4	−6.1	−36.2	−17.7	38.6	26.7
CO	Hong Kong	886.6	521.0	399.6	0.37	0.38	−365.6	−487.0	−41.2	−54.9	44.5	56.3
	Taiwan	0.47	0.26	0.29	0.17	0.08	−0.21	−0.18	−44.5	−39.1	44.7	39.5
Column CO	MOPITT	2.78	2.58	2.56	0.68	0.66	−0.19	−0.21	−6.9	−7.7	15.3	16.0
NO$_x$	Hong Kong	151.1	73.0	37.7	0.38	0.44	−78.1	−113.4	−51.7	−75.0	57.2	75.4
NO	Taiwan	4.58	2.95	3.04	0.07	0.09	−1.62	−1.53	−35.5	−33.5	68.9	69.4
NO$_2$	Hong Kong	66.4	56.2	32.3	0.38	0.42	−10.1	−34.0	−15.2	−51.3	42.3	57.1
	Taiwan	16.1	17.2	17.6	0.15	0.03	1.1	1.5	6.6	9.3	42.7	47.5
Column NO$_2$	SCIAMACHY	6.9	16.8	13.5	0.73	0.77	9.9	6.6	143.4	95.7	149.4	105.5
O$_3$	Hong Kong	40.5	45.2	68.9	0.56	0.62	4.6	28.3	11.5	69.8	67.9	86.7
	Taiwan	33.5	33.3	35.4	0.15	0.01	−0.14	1.88	−0.4	5.6	21.0	21.3
TOR	OMI/MLS	32.9	39.7	39.8	0.63	0.62	6.8	6.9	20.6	21.0	22.0	22.4
SO$_2$	Hong Kong	11.1	32.8	21.2	0.30	0.42	21.6	10.1	194.1	90.9	209.2	118.1
	Taiwan	4.04	1.15	1.56	0.34	0.32	−2.9	−2.48	−71.5	−61.4	74.5	67.3
Column SO$_2$	SCIAMACHY	0.43	0.54	0.57	0.49	0.47	0.11	0.14	25.4	33.4	66.0	72.1

[a] Units are the same for all variables in Table 2.

Desert. Predicted mineral dust particles are further transported into the downwind regions such as Shanxi, Hebei, Henan, and Shandong Provinces, leading to seasonal mean PM$_{10}$ concentrations as high as 200 µg m^{-3} over those regions. Although the model is able to reproduce the magnitude of PM$_{10}$ concentrations over many downwind sites, especially those in eastern and southeastern China, BASE largely overpredicts PM$_{10}$ over the dust source regions, which could be attributed to a few reasons. First, as shown in Section 3.1, BASE tends to overpredict the wind speed over the dust source regions, which may lead to the overestimation of dust emissions. Second, there are uncertainties associated with the API data. The API data for PM$_{10}$ has an upper limit of 500, which corresponds to daily average concentrations of 600 µg m^{-3}. This means all concentrations > 600 µg m^{-3} were recorded as 600 µg m^{-3} in the API data. The daily PM$_{10}$ concentrations have been reported to be much more than 1000 µg m^{-3} over the dust source regions (Li et al., 2011; Park et al., 2012) during the spring 2010 episode. By ignoring large PM$_{10}$ concentrations, the API data inevitably have lower PM$_{10}$ concentrations than those simulated by the model. Third, as reported in Wang et al. (2012), there exists uncertainties and limitations in the dust treatment used in this study. For example, the monthly variation of vegetation coverage is not considered in this work which might introduce uncertainties to dust emissions. The erodibility factor (E$_F$) in calculation of vertical dust fluxes is subjected to a range of values (i.e., 0.13–1.0). The value of 1.0 used in this work represents the

high end and thus might cause the overprediction of dust emissions.

Fig. 4b and c show the temporal variations of PM$_{10}$ at the two sites in Beijing and Tianjin (i.e., every 6-hr for Beijing and daily for Tianjin) between observations and simulations at various resolutions. The details of measurements over those two sites can be found in Han et al. (2012) and Bian et al. (2011), respectively. Generally, BASE across different resolutions is able to reproduce two major dust storm events on 3/19–20 and 3/22 that are also reported by previous studies (Bian et al., 2011; Li et al., 2011; Zhao et al., 2011; Han et al., 2012; Park et al., 2012) and capture the observed PM$_{10}$ variation during the measurement periods at both sites, although the model largely overpredicts PM$_{10}$ concentrations on 3/20 for both sites, indicating potential overestimation of dust emissions and excessive transport of dust from the source regions due to the overprediction of wind speed. The model sensitivity to grid resolutions for PM$_{10}$ is much higher during the dust storm events than non-dust storm events. Unlike the major meteorological variables as discussed in Section 3.1, the performance for PM$_{10}$ is not necessarily better at finer resolutions because a majority of dust source areas are only in D01 and the impacts of finer grid resolutions on dust emissions (major contributor to PM$_{10}$ concentrations) cannot be accurately assessed.

Fig. 5 shows the weekly variation of PM$_{2.5}$ and seasonal mean of PM$_{2.5}$ and its components (observations for components are only available for SO$_4^{-2}$, NH$_4^+$, and Cl$^-$) at two sites in Beijing (i.e., THU as

Table 4
Performance statistics of BASE for spring (March–May) 2010 over domain D03 (simulations over D01, D02, and D03 against observations over D03).

Variables[a]	Datasets	Mean Obs	Mean Sim			R			MB			NMB (%)			NME (%)		
			D01	D02	D03	D01	D02	D03	D01	D02	D03	D01	D02	D03	D01	D02	D03
T2	NCDC	11.38	10.1	10.3	10.33	0.98	0.99	0.99	−1.26	−1.07	−1.04	−11.0	−9.4	−9.2	12.9	10.5	10.2
Q2	NCDC	4.3	3.8	3.9	3.9	0.99	0.99	0.99	−0.47	−0.41	−0.37	−10.9	−9.5	−8.8	10.9	9.5	8.8
WS10	NCDC	3.06	3.46	3.34	3.19	0.16	0.14	0.18	0.40	0.28	0.13	13.1	9.1	4.2	28.6	27.9	26.9
WD10	NCDC	203.2	193.3	195.8	202.6	0.27	0.51	0.56	−9.9	−7.4	−0.6	−4.9	−3.6	−0.3	11.4	9.1	9.0
Precipitation	NCDC	0.88	0.84	0.83	0.91	0.58	0.69	0.66	−0.05	−0.05	0.03	−5.2	−6.2	3.6	55.2	53.8	55.3
	GPCP	0.7	0.9	0.9	1.0	0.22	0.22	0.23	0.22	0.25	0.32	31.6	35.2	45.6	81.1	85.2	90.9
	TMPA	0.93	0.92	0.95	1.02	0.75	0.73	0.67	−0.01	0.02	0.09	−0.9	1.8	9.6	18.6	19.1	22.5
SWDOWN	CERES	204.5	227.3	228.4	228.3	0.97	0.97	0.97	22.8	23.9	23.8	11.2	11.7	11.7	11.2	11.7	11.7
LWDOWN	CERES	296.1	286.2	285.6	285.6	0.99	0.99	0.98	−9.9	−10.5	−10.5	−3.3	−3.5	−3.6	3.4	3.7	3.7
SWCF	CERES	−48.0	−33.6	−32.7	−32.6	0.86	0.86	0.85	−14.5	−15.4	−15.4	−30.1	−32.0	−32.1	30.3	32.0	32.1
LWCF	CERES	30.4	23.2	22.5	22.7	0.50	0.38	0.33	−7.2	−7.9	−7.7	−23.8	−25.9	−25.4	23.9	25.9	25.5
OLR	CDC	224.0	226.5	227.3	227.0	0.92	0.90	0.90	2.5	3.3	3.0	1.1	1.5	1.3	2.5	2.9	2.9
AOD	MODIS	0.48	0.65	0.64	0.64	0.69	0.65	0.64	0.17	0.16	0.16	34.6	32.4	32.7	41.9	41.6	41.9
	AERONET	0.70	0.60	0.59	0.59	0.37	0.37	0.36	−0.10	−0.11	−0.11	−13.8	−15.1	−15.0	56.8	56.4	56.7
COT	MODIS	12.9	6.1	5.9	6.1	0.50	0.30	0.28	−6.8	−7.0	−6.8	−52.5	−54.3	−52.6	52.5	54.3	52.6
CF	MODIS	0.67	0.40	0.41	0.43	−0.19	−0.10	−0.07	−0.27	−0.25	−0.24	−39.8	−37.8	−36.0	39.8	37.8	36.0
CCN	MODIS	4.67	1.39	1.56	1.54	−0.39	−0.36	−0.35	−3.28	−3.11	−3.13	−70.2	−66.7	−67.1	70.2	66.7	67.1
CDNC	MODIS	161.4	127.7	159.9	154.2	−0.10	−0.10	−0.10	−33.7	−1.5	−7.2	−20.9	−0.9	−4.5	57.4	59.7	60.6
LWP	MODIS	86.3	25.7	24.3	24.9	0.67	0.49	0.48	−60.5	−61.9	−61.4	−70.2	−71.8	−71.1	70.2	71.8	71.1
IWP	MODIS	191.0	17.6	17.3	17.9	−0.31	−0.21	−0.21	−173.5	−173.8	−173.1	−90.8	−91.0	−90.6	90.8	91.0	90.6
PWV	MODIS	1.06	1.08	1.07	1.07	0.98	0.98	0.97	0.01	0.01	0.01	1.2	0.6	0.7	7.5	7.8	8.1
PM$_{10}$	China	111.1	164.0	168.0	163.1	0.05	0.04	0.05	52.9	56.9	52.1	47.6	51.2	46.9	51.5	55.6	50.6
Column CO	MOPITT	3.15	3.03	3.00	3.02	0.76	0.76	0.72	−0.12	−0.15	−0.13	−3.8	−4.7	−4.3	8.7	9.2	9.7
Column NO$_2$	SCIAMACHY	24.0	37.0	32.4	31.9	0.60	0.70	0.67	13.0	8.3	7.9	54.0	34.7	32.8	58.8	43.4	43.0
TOR	OMI/MLS	32.2	38.9	39.0	39.0	0.66	0.62	0.62	6.7	6.8	6.8	20.7	21.1	21.1	21.3	21.7	21.8
Column SO$_2$	SCIAMACHY	0.73	1.19	1.26	1.26	0.11	0.10	0.09	0.47	0.53	0.53	64.0	73.0	72.9	71.6	79.8	80.1

[a] Units are the same for all variables in Table 2.

a suburban site and Miyun as a rural site). Overall the model predicts weekly variation of PM$_{2.5}$ better over the THU site than Miyun. PM$_{2.5}$ is dominated by dust particles (representing by OIN) and OC during the measurement period at both sites. The performance differences to grid resolutions is much more apparent for PM$_{2.5}$ concentrations (Fig. 5) compared to PM$_{10}$ (Fig. 4b and c), with the highest concentrations at a 4-km resolution and the lowest concentrations at a 12-km resolution at both sites. At THU, the simulation at the 4-km resolution gives the best performance most of time except for 4/9-4/30 when the simulation at

the 12-km resolution performs the best and both 12-km and 36-km resolutions largely underpredict PM$_{2.5}$. At Miyun, the simulation at the12-km resolution predicts PM$_{2.5}$ concentrations that are the closest to observations during most of time and the simulation at the 4-km resolution performs the worst with large overpredictions most of time.

Tables 2–4 summarizes the domain-average statistics for all the major chemical variables evaluated in this work against various surface and satellite datasets in D01, D02, and D03, respectively, for BASE and also show the performance sensitivity to different grid resolutions by
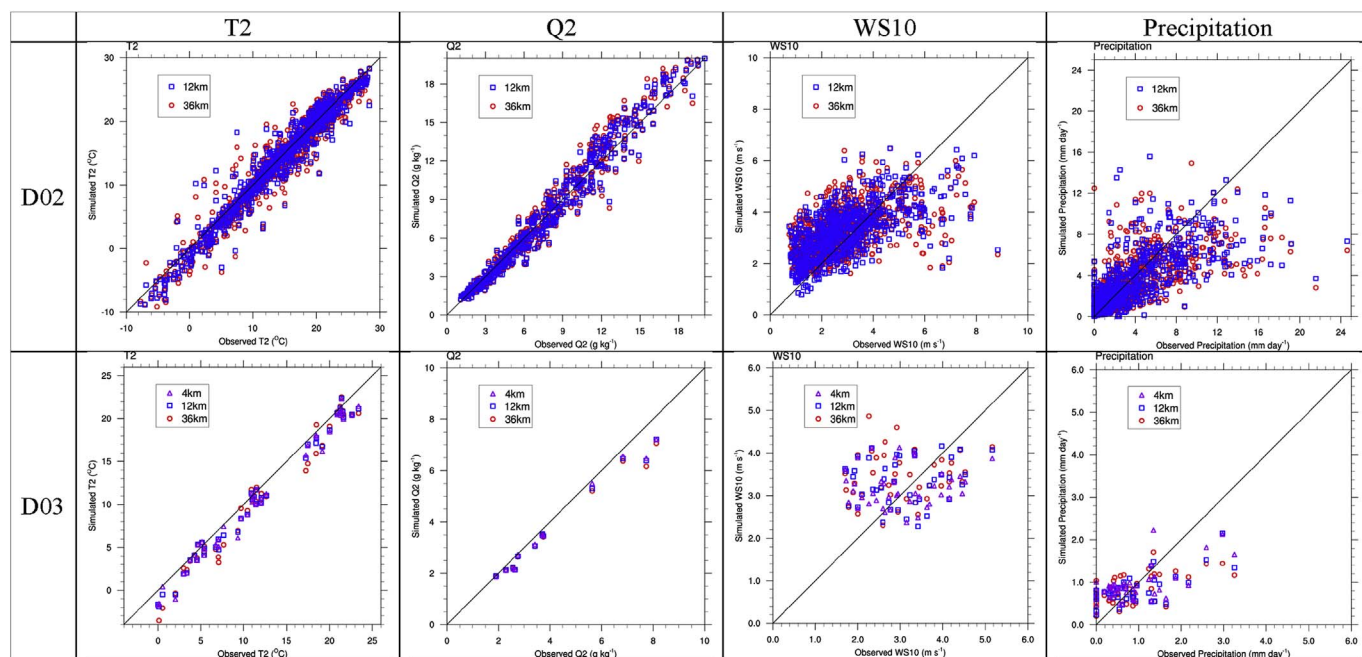
Fig. 2. Scatter plots of seasonal mean observed and simulated T2, Q2, WS10, and precipitation (from left to right) over individual sites (represented by individual dots) of NCDC for BASE in D02 and D03 for spring 2010.
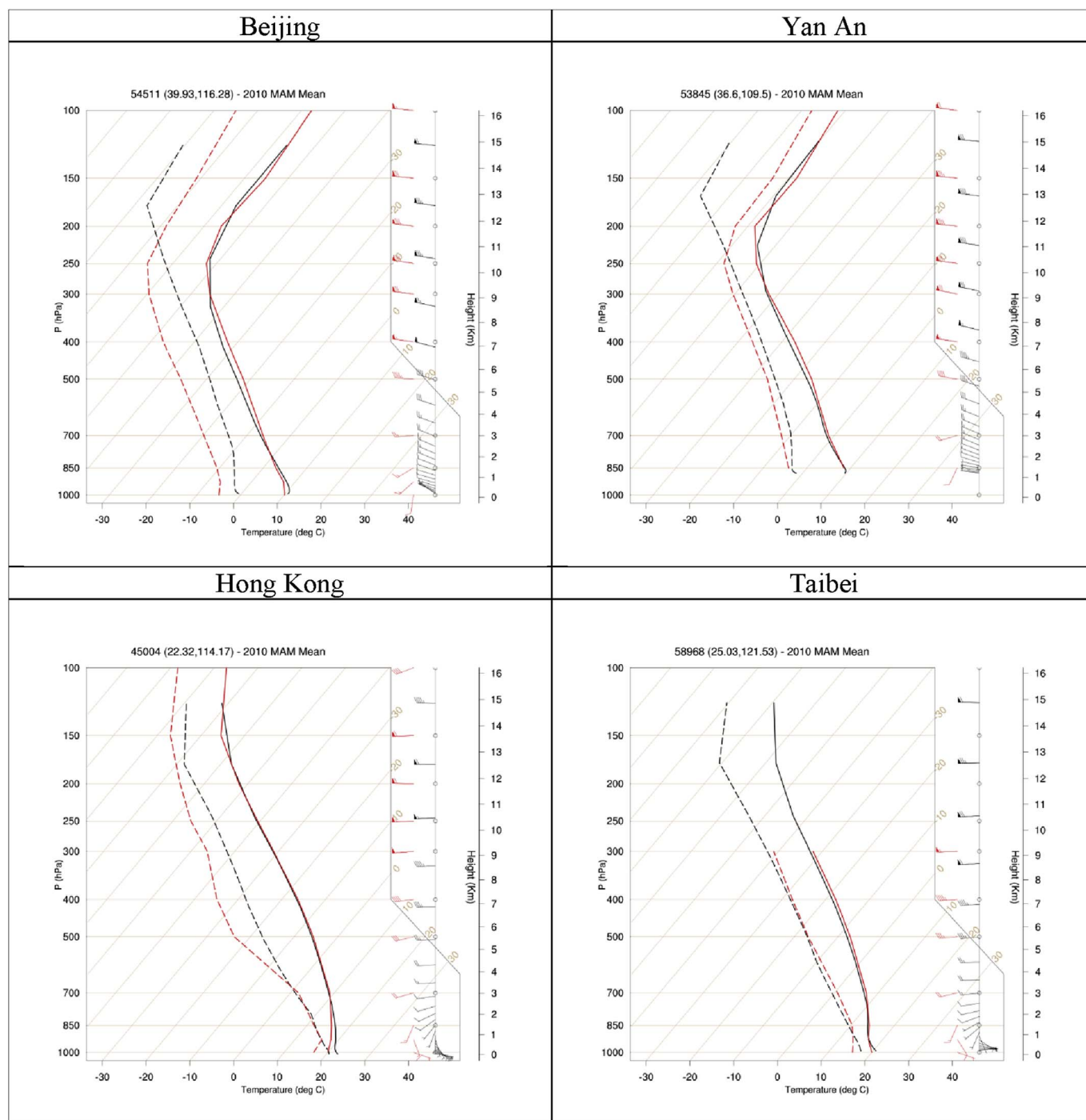
Fig. 3. Seasonal mean observed and simulated skew-T plots of temperature (red and black solid lines, respectively), dew point temperature (red and black dash lines, respectively), and wind speed and direction (red and black staffs and attached barbs, respectively; the triangle, long barb and a short barb perpendicular to the overall staff representing 50, 10 and 5 knots, respectively) at four selected sites (i.e., Beijing, Yan An, Hong Kong, and Taibei) in D02 or D03 for BASE. (For interpretation of the references to colour in this figure legend, the reader is referred to the Web version of this article.)

using the same common data for different resolutions (Tables 3 and 4). In D01, BASE predicts surface O_3 and NO_2 well with NMBs within ± 15% in Hong Kong, Taiwan, and South Korea and less than −20% in Japan. The model predicts $PM_{2.5}$ and PM_{10} reasonably well with NMBs typically within ± 30% in mainland China, Hong Kong, and Japan, considering the higher benchmark values recommended by the U.S. EPA (US EPA, 2007) for model evaluation of $PM_{2.5}$ compared to O_3 (i.e., NMB of ≤ ± 15% and ± 30% for O_3 and $PM_{2.5}$, respectively). However, BASE largely underpredicts CO, NO, NO_x, and SO_2 against most datasets. The relatively poor performance for those variables is overall

consistent with Zhang (2014) and can be largely attributed to uncertainties associated with the emission inventory and the emission vertical distributions for CO, NO, and SO_2. As shown in Tables 3 and 4, the use of 12-km resolution leads to better performance for most variables such as PM_{10} in mainland China and Taiwan, $PM_{2.5}$ in Hong Kong and Taiwan, CO in Taiwan, and SO_2 in Hong Kong and Taiwan in terms of NMBs, NMEs, and Rs compared to the 36-km resolution. Furthermore, the 4-km resolution yields the best performance for PM_{10} and NO_2, despite limited datasets are available to evaluate the simulations in D03.
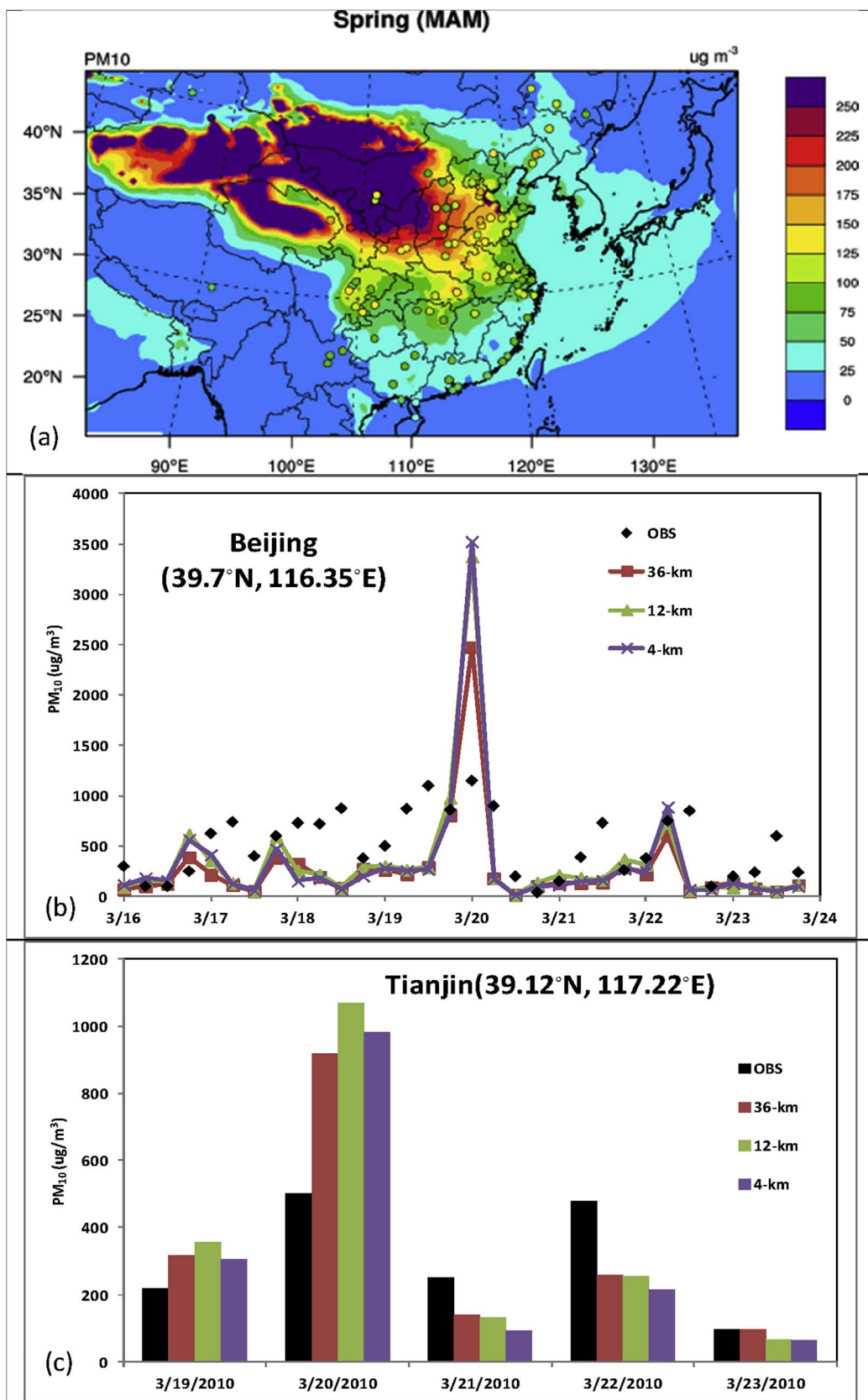
Fig. 4. (a) Simulated seasonal mean PM_{10} concentrations overlaid with observations from API in D01; (b) observed and simulated every-6 hr PM_{10} concentrations at a site in Beijing in D01, D02, and D03; (c) observed and simulated daily PM_{10} concentrations at a site in Tianjin in D01, D02, and D03 for BASE.

The comparison also shows the use of finer grid resolutions in this study does not necessarily outperforms the coarser resolution nor it shows significant improvements for all chemical species, which is consistent with some previous studies (Queen and Zhang, 2008; Fountoukis et al., 2013; Zhang et al., 2013; Kuik et al., 2016). As indicated by Zhang et al. (2013) and Kuik et al. (2016), the potential worse performance of simulations with finer resolutions for chemical species could be due to the nonlinear interactions between meteorology
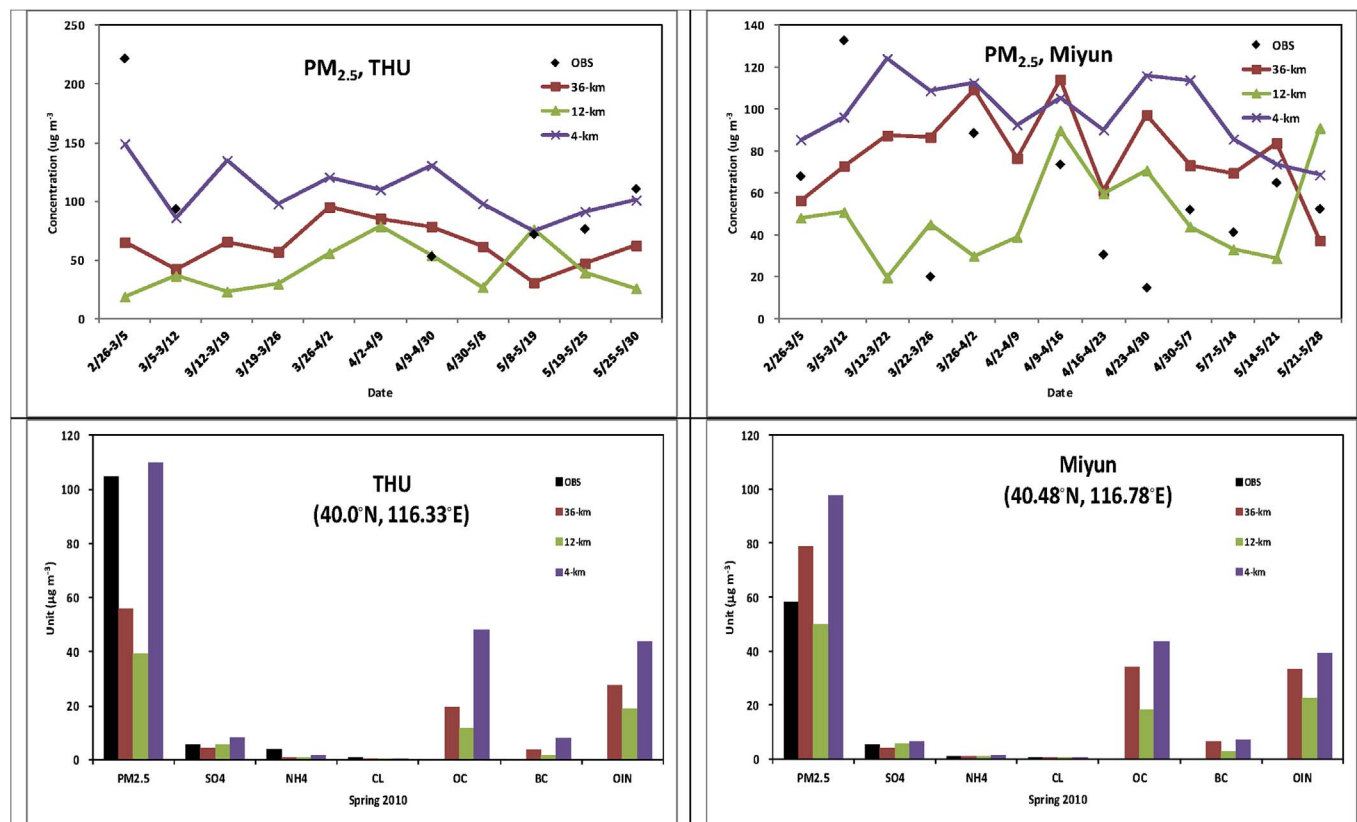
Fig. 5. Observed and simulated daily time series and seasonal mean PM$_{2.5}$ and its component concentrations at two sites in Beijing: Tsinghua (THU) and Miyun, respectively, in D01, D02, and D03 for BASE.

and chemistry and their responses to grid resolutions and higher uncertainties associated with the model inputs (e.g., emissions) or parameters at the finer grid resolutions. In addition, the grid-averaging effects of land use data and emissions at a coarser grid resolution may sometime smooth out uncertainties of model predictions and therefore result in better agreements with observations.

3.3. Radiation and cloud associated variables

Fig. 6 shows the spatial differences between simulation BASE and MODIS retrievals for CCN at supersaturation of 0.5% (observations only available over the ocean), CDNC, CF, and COT in D02 for spring 2010. As shown, BASE largely underpredicts CCN along the coastlines, especially over the Bohai Bay and eastern China coastal areas, due to underpredictions of aerosols over those regions (See Table 3) or high uncertainties associated with CCN retrievals especially under polluted marine environments (Andreae, 2009). The model also moderately overpredicts CDNC in widespread areas of eastern and southeastern China and Koreas while largely underpredicts CDNC in other regions. CF is relatively well predicted with the lowest biases over southeastern China. The spatial variation of model biases for COT and LWP (figure not shown) are similar with both showing moderate overpredictions in southeastern China and large widespread underpredictions over the rest of the domain. The underpredictions of COT and LWP are more consistent with the underprediction of CDNC. As reported by Lim et al. (2014), the inclusion of cloud microphysics and aerosol-cloud interactions in the new ZM cumulus scheme in the current version of WRF-CAM5 may generate much higher total cloud liquid water. The overprediction of LWP in the above region could indicate the excessive predicted cloud liquid water, which may also lead to positive biases of COT.

The model sensitivity to grid resolutions for selected radiation variables (i.e., SWDOWN, LWDOWN, SWCF, and AOD) is further

examined in Fig. 7 and Fig. S6–S7. BASE with grid resolutions of both 12-km and 36-km shows similar widespread overprediction of SWDOWN in D02. The model biases of SWDOWN over the southern part of the domain are mainly due to large underpredictions of AOD as shown in Fig. 7, while those over the northern part of the domain are more likely to be related to underpredictions of LWP and COT as shown in Fig. 6. Relatively large underpredictions of LWDOWN occur over the northern part of the D02 domain, which are also associated with underpredictions of cloud variables over the same region. There are also widespread underpredictions of SWCF across the domains, which is related to the negative biases of cloud fraction and COT. Large overprediction and underprediction of AOD also occur over the northern and southern parts of the domain, respectively, mainly due to potential overprediction of dust concentrations in northern source and downwind areas as discussed in Section 3.2 and underprediction of aerosols over the southern areas as shown in Tables 2 and 3. As shown in Fig. 7 and Fig. S6, the simulation at a finer grid resolution (i.e., 12-km vs 36-km) does not show superior performance for major radiation variables despite showing more detailed spatial variations. The domain-average statistics for radiation and cloud variables in both D02 and D03 are further summarized in Tables 3 and 4. Similar to the simulation with 36-km resolution, 12-km shows overall good performance for SWDOWN, LWDOWN, OLR, COT, CF, CDNC, and PWV, moderate performance for SWCF, LWCF, AOD, and LWP, respectively, and poor performance (large underpredictions) for CCN and IWP. The performance for 4-km resolution is generally comparable to but not superior to 36-km and 12-km resolutions. The large underpredictions of cloud variables could be in part due to the underpredictions of aerosol concentrations and more possibly the uncertainties associated with aerosol activation treatment and cloud schemes.
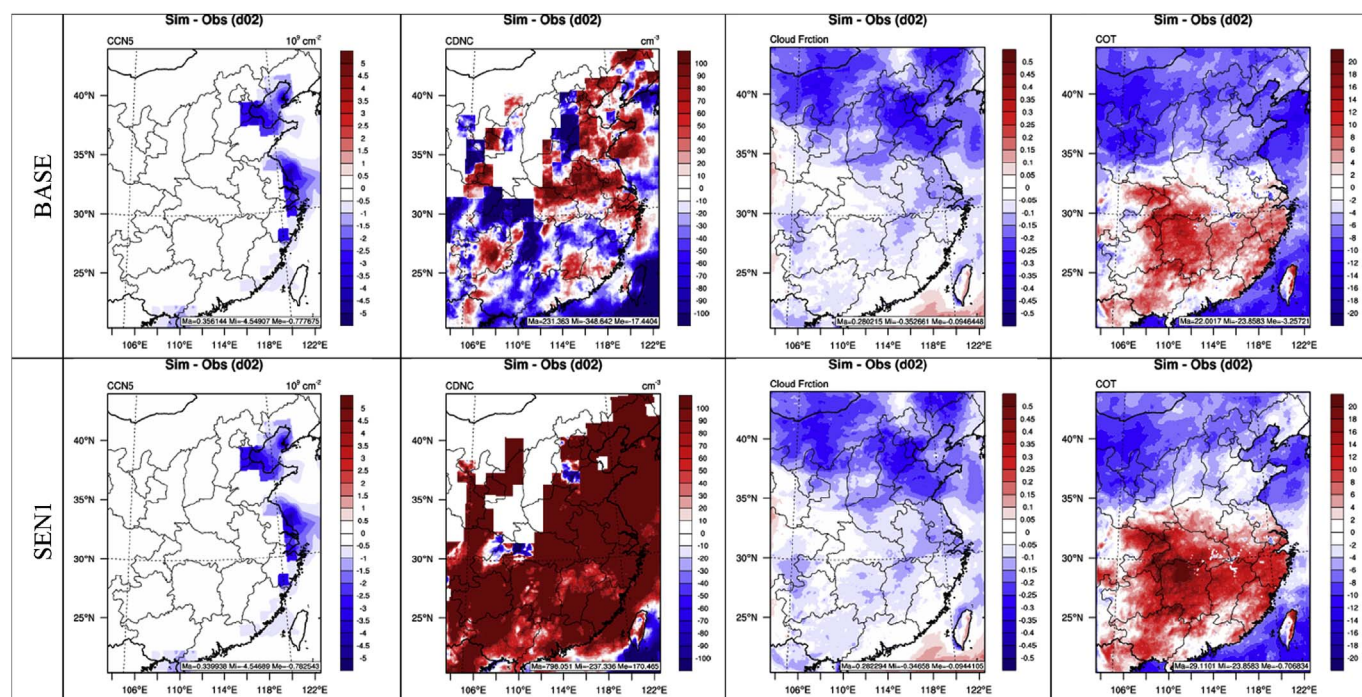
Fig. 6. Spatial differences between seasonal mean simulation and observations for CCN at S = 0.5%, CDNC, CF, and COT (from left to right) for BASE and SEN1 in D02 for spring 2010.

4. Sensitivity studies

4.1. Impacts of different aerosol activation parameterizations

4.1.1. Performance comparison against observations

Fig. 6 also shows the spatial differences between SEN1 and MODIS retrievals for CCN at supersaturation of 0.5%, CDNC, CF, and COT in D02 to compare model performance between SEN1 and BASE. As shown, SEN1 gives much higher widespread overprediction of CDNC over land and changes performance from underprediction to overprediction over large areas of domain. The much higher CDNC predictions by SEN1 might be due to two reasons. One reason is associated with the much higher activation fractions in low altitude warm clouds for the accumulation mode particles by FN05 as reported by Zhang et al. (2015a). Another reason might be associated with the dust adsorptive activation in K09 in the FN series scheme. It is found in Section 4.2 that adsorptive activation from dust particles may contribute significantly to the increase of total CDNC (~45%) between the FN and AG00 schemes. Large overprediction of dust concentrations as indicated in Section 3.2 may further lead to the overprediction of CDNC by SEN1, especially over northern part of domain. The increases of CDNC from SEN1 further slightly increase CF and moderately increase COT, which in turn deteriorate the performance of COT over southeastern China and improve the performance of COT and CF over rest of the domain compared to BASE. As shown in Tables 2–4 and Tables S3–S5, SEN1 shows performance improvements against BASE at different resolutions for most cloud variables with, for example, domain-average NMBs of −24.5% vs. −35.8% for COT, −10.0% vs. −10.6% for CF, and −34.3% vs −47.5% for CWP, respectively, in D01. The improvements for COT, CF, and CWP further lead to better performance for major radiative variables and precipitation in SEN1 vs. BASE. The impacts of the FN series schemes on other meteorological and chemical variables in terms of statistics are relatively small due to the smaller effects of aerosol activation on those variables through feedbacks.

Fig. 8 shows meridional mean time series plots for precipitation in D03 at resolutions 36-, 12-, and 4-km, respectively, compared with TMPA observations between BASE and SEN1. The time period on the x-axis covers Julian Days 60–151 (i.e., from March 01 to May 31, 2010).

As shown, BASE across different resolutions is able to capture all the major precipitation events (e.g., on Julian Days 70–75, 99–104, 120–126, and 134–139) during the simulation time period, despite some biases in terms of precipitation amounts and locations. For example, BASE overpredicts precipitation between 37.6 and 39.6 °N during Julian Days 70–75 and underpredicts it between 40.2-41.2 °N and 37.6–39.6 °N during Julian Days 120–126. The overall performance for precipitation at finer grid resolutions (e.g., 4-km) is slightly better than coarser resolution, especially for the heavy rain event during Julian Days 120–126. The performance of SEN1 across different resolutions is generally comparable to BASE for most of the time periods except during Julian Days 120–126, when SEN1 predicts much higher precipitation than BASE and shows generally better agreement with observations. The results here indicate that the impacts of different aerosol activation parameterizations on precipitation are more significant than those of grid resolutions.

4.1.2. Impacts on cloud/radiation and air quality

Fig. 9a and b show the differences between SEN1 and BASE for CDNC, COT, LWP, precipitation, SWDOWN, T2, PBL height, and WS10 in D03 to demonstrate the impacts of the FN series aerosol activation schemes on meteorology and aerosol-cloud interactions (Figs. S8–S10 shows similar results for other domains). As expected, CDNC predicted by SEN1 using the FN aerosol activation scheme is much higher than BASE in D01 with increases by up to $10.5 \times 10^4 \, cm^{-3}$ (> 100%), especially over the eastern part of domain where atmospheric moisture are high. The increase of CDNC in turn increases COT by up to 3.6 (18.8%) and LWP by up to $18.0 \, g \, m^{-2}$ (33.2%), and increases cloud cover (not shown) that decreases SWDOWN by up to $7.5 \, W \, m^{-2}$ (3.2%). The aforementioned changes further decrease T2 by up to 0.3 °C (> 100%) and PBL height by up to 30.7 m (6.7%) through the indirect cloud-radiation feedbacks. Precipitation mainly increases in D03 where cold clouds are dominant, which is consistent with other modeling studies (e.g., Lim et al., 2014). The domain-average precipitation is increased by $0.1 \, mm \, day^{-1}$ (10%), due to the increase of LWP (Zhang et al., 2015a).

The impacts of the FN series aerosol activation schemes on air quality in D03 is further examined in Fig. 9c for major air pollutants
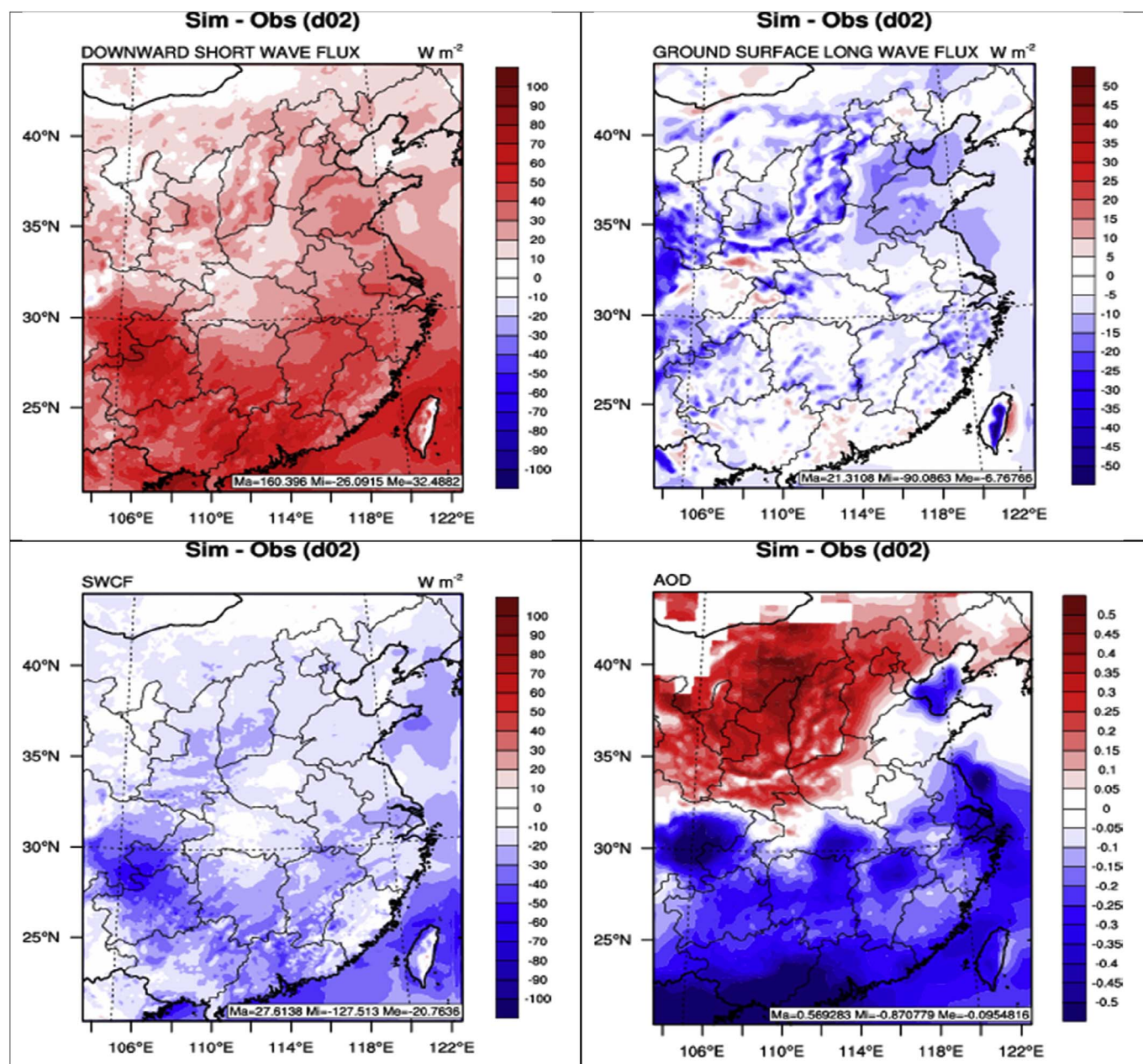
Fig. 7. Spatial differences between simulation and observations for SWDOWN, LWDOWN, SWCF, and AOD (from top to bottom) for BASE in D02 for spring 2010.

such as O_3, NO_2, SO_2, and $PM_{2.5}$. The air pollution is the most severe in China over the Beijing-Tianjin-Hebei area in D03 of this study. The mixing ratio of O_3 decreases over most areas of D03 by up to -2.0 ppb (-9.0%), which is consistent with the reduction of solar radiation and T2 caused by aerosol-cloud interactions. The increases of NO_2 mixing ratios by up to 0.7 ppb (4.0%) in D03 are mainly due to the decrease of its photolytic rate, which also contributes to the decrease of O_3 through the chemical titration. The SO_2 mixing ratio decreases over the large area of the northern domain by up to -1.5 ppb (-5.0%), mainly caused by the increase of PBLH and wind speed over the same areas. Large decrease of $PM_{2.5}$ by up to $-8.0\,\mu g\,m^{-3}$ (-7.0%) occurs over Beijing and Tianjin areas mainly due to the reduced BC and POA caused by the increased dispersion (increase of PBL height and wind speed) over the same area. The above results show moderate improvements of the FN series scheme in air quality simulation in the heavily polluted area and thus indicate the importance of inclusion of the FN series in the model.

4.2. Impacts of adsorptive activation of dust particles

In this section, the impacts of adsorptive activation of dust particles on the simulations are further examined in D03. In addition, the simulation results from SEN1 and SEN2 in D03 are split into two shorter time periods, including the dust storm period (when the maximum dust concentrations over the domain are more than $200\,\mu g\,m^{-3}$; 33 days in total) and non-dust storm period (59 days in total). The domain-average concentrations of fine-mode dust between dust and non-dust storm periods are 59.9 vs. $21.1\,\mu g\,m^{-3}$, respectively, while the aerosol concentrations without dust are more comparable (i.e., 33.5 vs. $36.6\,\mu g\,m^{-3}$) (see Fig. S11).

Figs. 10–12 show the differences between SEN1 and SEN2 for similar cloud, meteorological, and air quality variables as shown in Fig. 9 to demonstrate the impacts of the adsorptive activation of dust particles treated in the FN series parameterization on those variables. As shown, the inclusion of dust particles to aerosol activation increases the CDNC over the domain as expected but to a lesser extent than the impact of
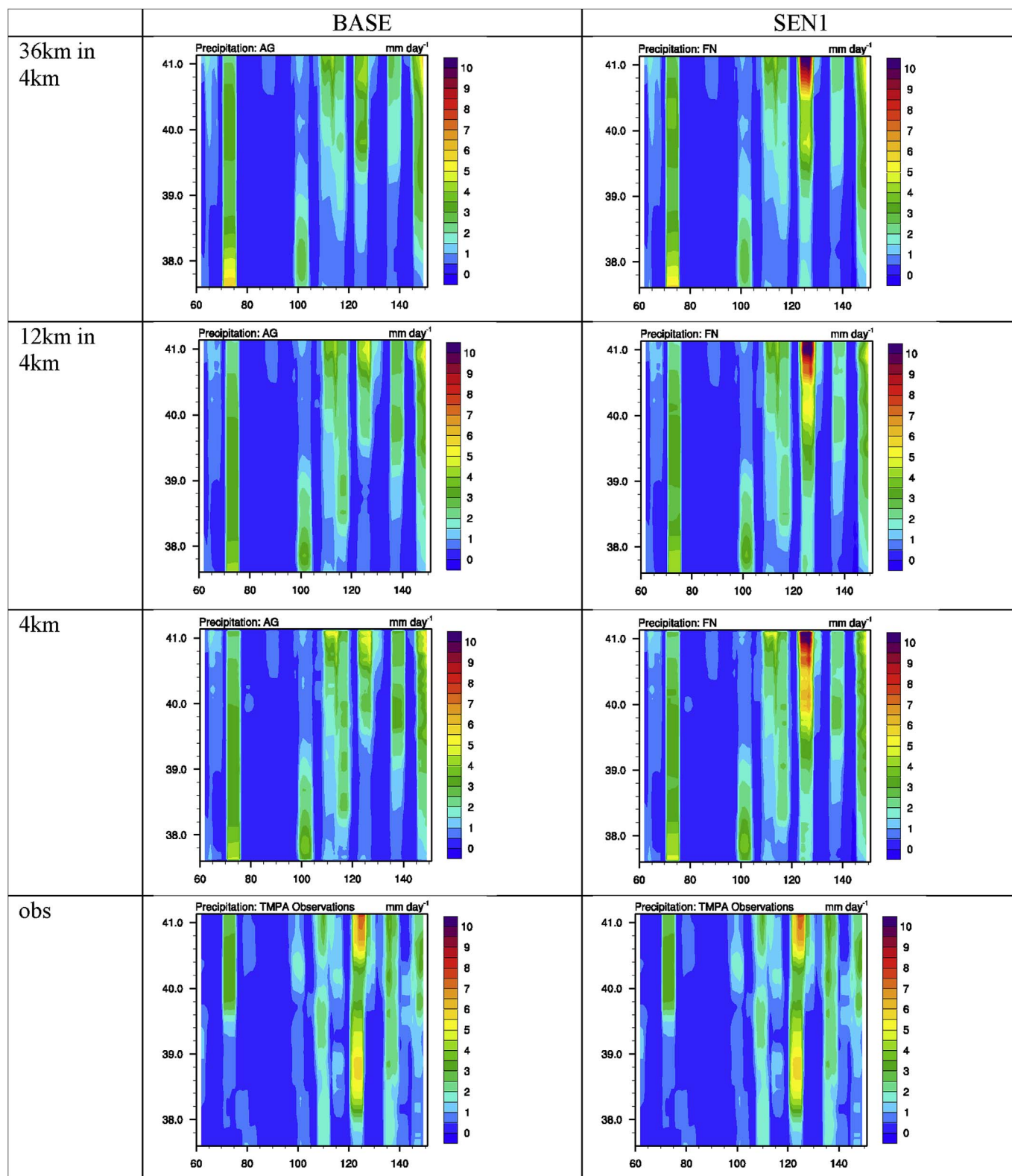
Fig. 8. Time-series-meridional analysis of BASE and SEN1 over the 36-in-4 km, 12-in-4 km, and 4 km domains (results from coarser domain are remapped finer domain by applying the bilinear weighted interpolation) compared against the TMPA observations. Values represent 5-day running averages. Time period on the x-axis pertains to Julian Day 60–151 (March 01 – May 31, 2010).

changing the aerosol activation parameterization from AG to FN05 series (Fig. 9a). The adsorptive activation of dust particles may contribute roughly 45% of increase of CDNC (the domain-average of 2.6 vs. $5.8 \times 10^4 \, \mathrm{cm}^{-3}$ between SEN1-SEN2 and SEN1-BASE) in D03, which is consistent with the range reported by Karydis et al. (2011). The

increases of CDNC also increase COT and LWP and generally decrease precipitation. In contrast to Fig. 9b, larger areas of increase of SWDOWN and T2 over the western part of D03 occur, which is due to the decrease of AOD (figure not shown). The decrease of SWDOWN and T2 over the eastern and southeastern part of D03 is due to the large
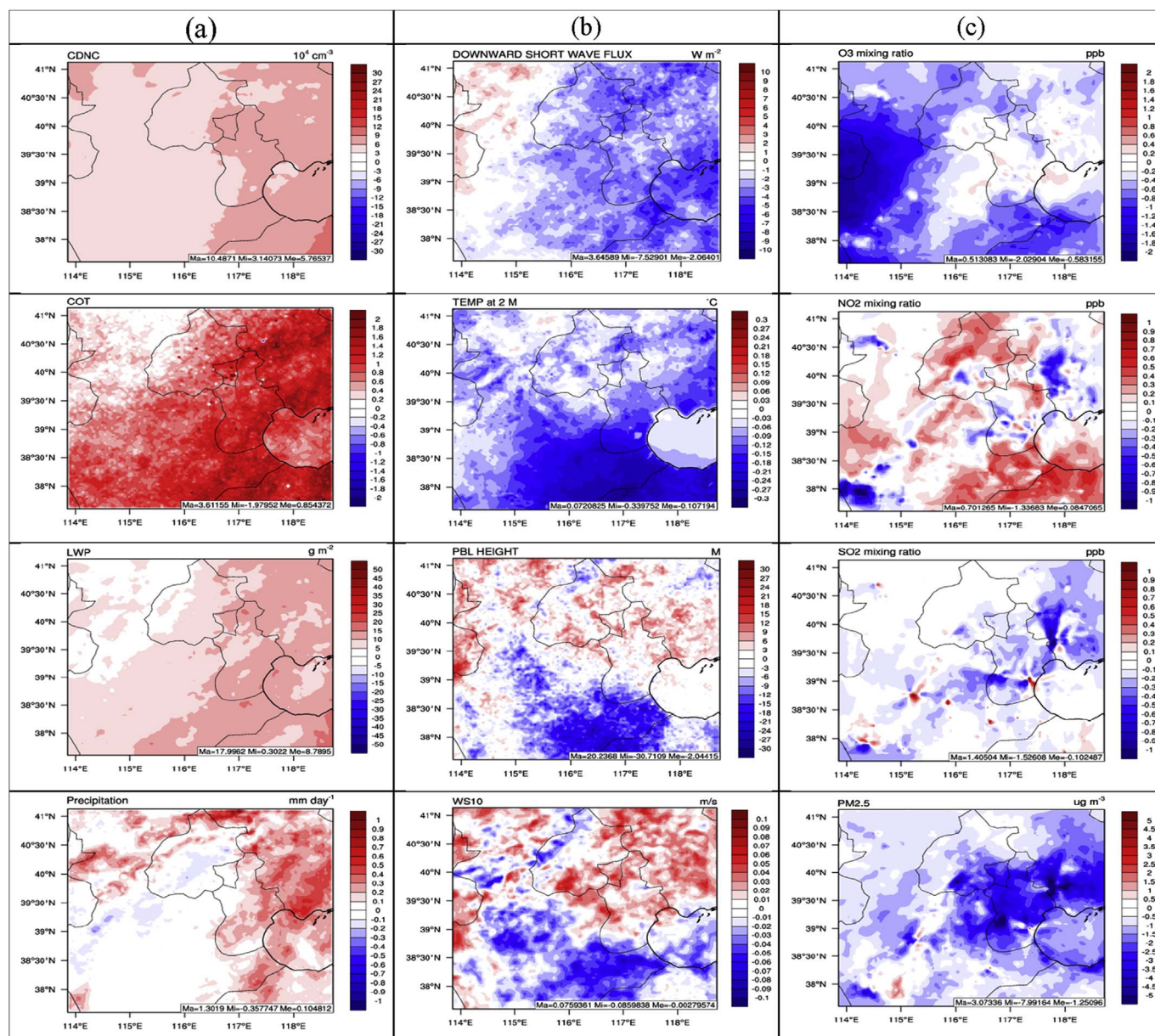
Fig. 9. Differences of seasonal mean between SEN1 and BASE (FN-AG) for a) left panel: CDNC, COT, LWP, and precipitation (from top to bottom); b) center panel: SWDOWN, T2, PBL height, and WS10 (from top to bottom); c) right panel: O_3, NO_2, SO_2, and $PM_{2.5}$ (from top to bottom) in D03 in spring 2010.

increase of cloud cover (figures not shown). PBL height and WS10 also largely increase especially over the western part of D03 through the aerosol semi-effects caused by the increase of SWDOWN and T2. As shown, the impacts of adsorptive activation of dust particles on those major cloud and meteorological variables are generally larger during the dust storm periods than non-dust storm periods especially for CDNC, COT, LWP, precipitation, and PBL height. For example, the decrease of precipitation due to adsorptive dust activation may reach up to 1.64 mm day^{-1} during dust storm periods compared to only 0.56 mm day^{-1} during non-dust storm periods. The impacts on SWDOWN and T2 are more complicated, with opposite changes for T2 caused by complex aerosol semi-direct effects. As shown in Fig. 12, the impacts of adsorptive activation of dust on air quality are more complicated than those shown in Fig. 9c over the whole time period. The O_3 mixing ratios decrease in the northwestern and southeastern areas of D03 but they increase in the central area over Beijing and Tianjin. The decrease in the northwestern region is mainly due to the large increase of PBL height while the decrease in the southeastern region and increase in the

central region are determined by the decrease or increase of SWDOWN and T2 over those areas. The changes of NO_2 show the opposite pattern as O_3 which indicates the dominant impacts of O_3 titration. The increase of O_3 especially over the central domain leads to the large decrease of SO_2 caused by more oxidation. The domain-average decrease of $PM_{2.5}$ is more dominated by the increase of dispersion caused by increasing PBL height. Unlike cloud variables, the impacts on air quality seem to be more complex (sometimes with opposite trends) between dust and non-dust storm periods due to complex aerosol effects under different levels of anthropogenic air pollutants between two periods (e.g., the anthropogenic air pollutants are generally higher during non-dust period).

Fig. 13 shows zonally-averaged cross-section plots for total dust concentrations, changes (SEN1-SEN2) of activation fraction (in percentage) of dust, changes of CDNC, and changes of LWP, respectively, due to adsorptive dust activation during the dust and non-dust storm periods in D03 in spring 2010. As expected, dust concentrations are much higher during dust periods than non-dust periods. The dust
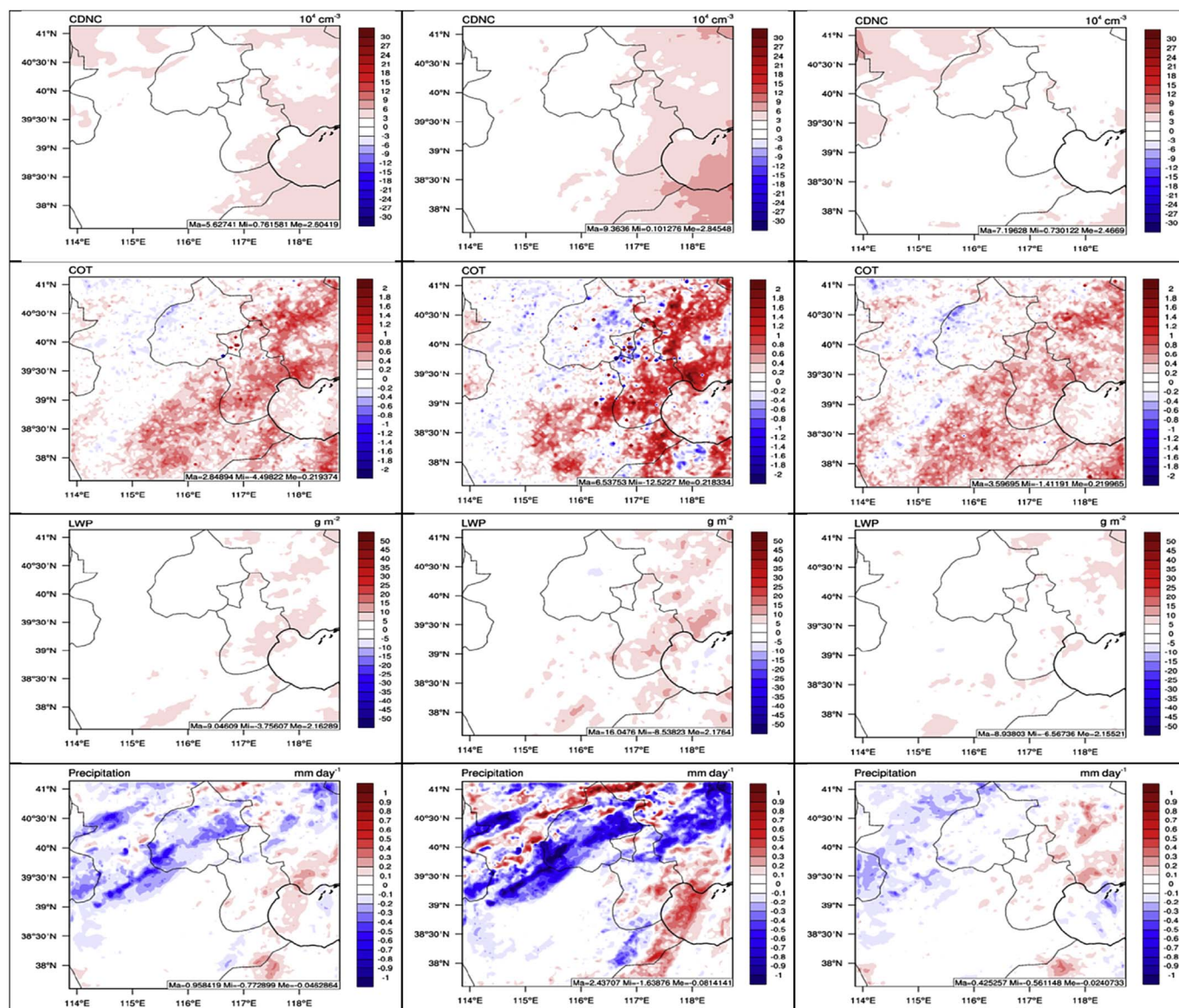
Fig. 10. Differences between SEN1 and SEN2 (FN-FN no dust activation) for CDNC, COT, LWP, and precipitation (from top to bottom) during the whole period (left panel), dust period (center panel), and non-dust period (right panel) in D03 in spring 2010.

concentrations peak in the lower troposphere at around 850 hPa during dust periods and at around 800 hPa during non-dust periods, which is consistent with previous studies on the Asian dust transport pathways (Wang et al., 2012). High dust concentrations also occur in the southern part of the domain, indicating the northward transport pathway in D03, which is consistent with the finding of Zhang et al. (2003). The changes of activation fraction between SEN1 and SEN2 are generally comparable between different dust periods with slightly higher increase during the dust storm periods. Increases of activation fraction for both periods peak (> 50%) between 850 and 500 hPa, which lead to large increase of CDNC as shown in the same figure. There is another peak for increases of CDNC for both periods near the surface layers, which could be caused by moderately high dust concentrations and higher atmospheric moisture near the surface layers. The height of the peaks of increases of CDNC gradually decreases towards the north, which aligns well with the changes of moisture profiles. Increases of CDNC during dust episodes are also larger than non-dust episodes mainly due to the adsorptive activation of more dust particles, which is consistent with Fig. 10. The increases of CDNC also further increase LWP through microphysics processes as discussed before.

5. Conclusions

In this study, triple-nested simulations across 36-, 12-, and 4-km horizontal grid resolutions using the online-coupled regional climate/air quality model WRF-CAM5 have been conducted to investigate the model performance at various grid resolutions especially for the fine scales for major meteorological, chemical, and radiation/cloud variables and the impacts of different aerosol activation parameterizations on regional climate and air quality. To achieve the goal of this work, three sets of simulations have been conducted including BASE using the default aerosol activation scheme (i.e., AG00), SEN1 using the updated aerosol activation scheme (i.e., FN series), and SEN2 using the same FN series scheme but excluding the adsorptive activation of dust particles treatment.

Model evaluation of BASE against surface, radiosonde, and satellite datasets shows that WRF-CAM5 can reproduce major meteorological and radiation variables very well especially for T2, Q2, WS10, WD10, SWDOWN, LWDOWN, and OLR with the domain-average NMBs typically within ± 15% across different grid resolutions. However, the model grossly overpredicts precipitation against different datasets at
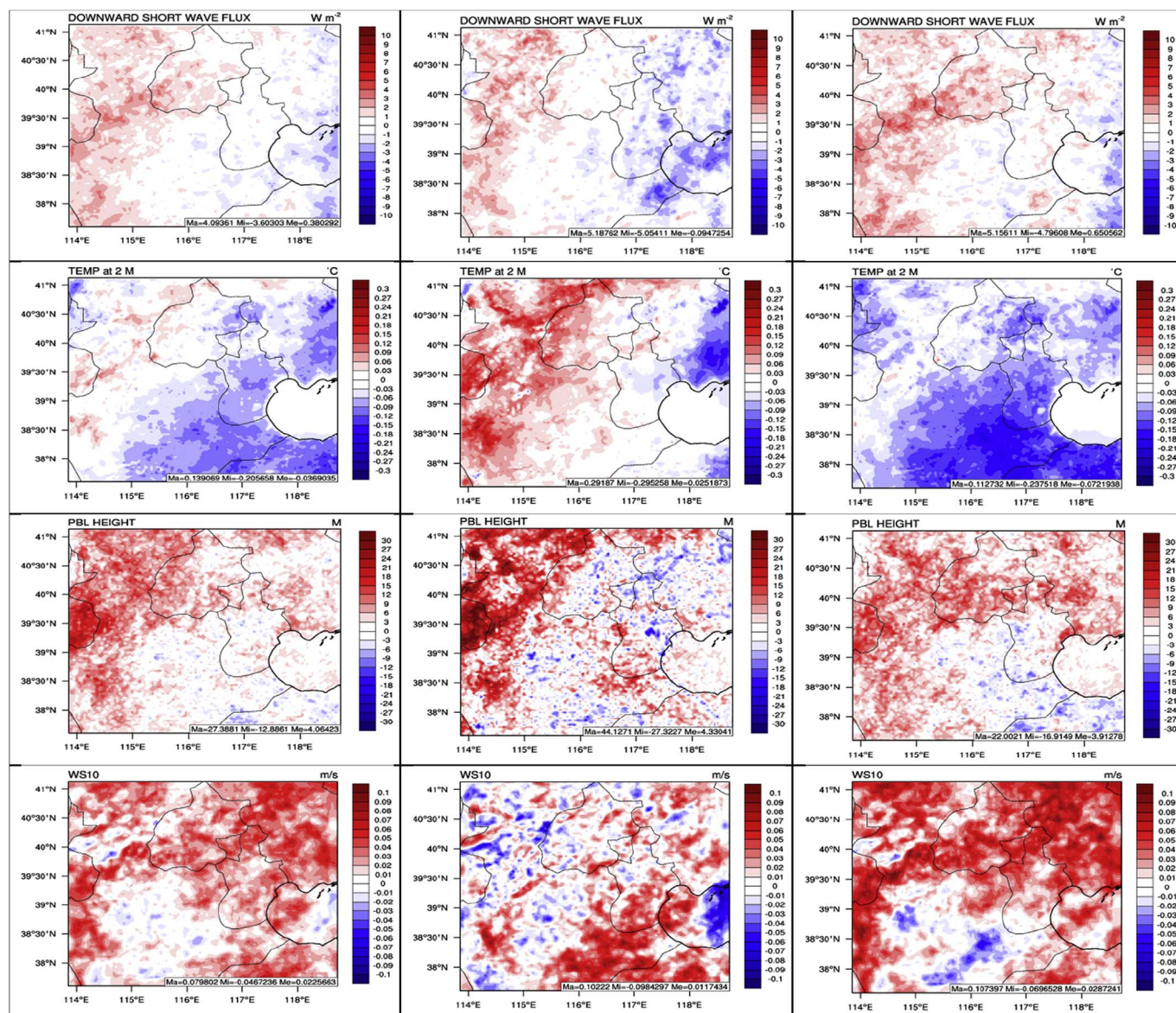
Fig. 11. Differences between SEN1 and SEN2 (FN-FN no dust activation) for SWDOWN, T2, PBL height, and WS10 (from top to bottom) during the whole period (left panel), dust period (center panel), and non-dust period (right panel) in D03 in spring 2010.

the 36-km resolution, which might be caused by a few factors including uncertainties associated with the microphysics scheme (i.e., the Morrison scheme in the work) and the land surface scheme (i.e., the NOAH scheme) and the missing cloud-radiation feedbacks for the convective cloud in the current version of model. The model performance for chemical variables is mixed, depending on the species. BASE captures a few major dust storm events by reproducing the observed PM_{10} concentrations from various datasets, which have also been reported by previous studies (Bian et al., 2011; Li et al., 2011; Zhao et al., 2011) despite some potential overestimation of dust emissions caused by overprediction of wind speeds in the source regions and uncertainties in the dust emission scheme. The model also reproduces the observed surface O_3, NO_2, $PM_{2.5}$, PM_{10}, column CO and SO_2, and TOR reasonably well with NMBs typically between ± 15% and ± 30%, although giving worse performance for surface NO, SO_2, and column NO_2. For radiation and cloud variables, BASE shows good performance for shortwave and longwave radiation, CF, and PWV with domain-average NMBs of within ± 15% and moderately or significantly underpredicts variables such as AOD, COT, CCN, CDNC, and LWP with NMBs typically > ± 30% across all grid resolutions. The large

underpredictions for those variables are partially due to the under-predictions of aerosol concentrations and more possibly high uncertainties associated with the model treatments of aerosol activation and aerosol-cloud interactions.

The model performance sensitivity to horizontal grid resolutions is further examined through analysis of temporal variation and domain-average statistics of major meteorological, chemical, and radiation/cloud variables. In general, WRF-CAM5 at a finer resolution gives better performance for T2, Q2, WS10, and WD10 and major surface chemical species (except those over Hong Kong) than coarser resolution in terms of both temporal variation and statistics performance. However, some chemical variables and variables associated with aerosol-cloud interaction from the finer resolutions are only comparable and not necessarily superior to coarser resolutions. For example, the predictions of domain-average COT and LWP and many chemical variables in Hong Kong are worse at 12-km compared to 36-km resolution. The 4-km predictions only give noticeably better performance for surface PM_{10} and column NO_2 (partially due to lack of surface measurements). Overall, the model performance comparison across different resolutions shows encouraging results for major surface meteorological and
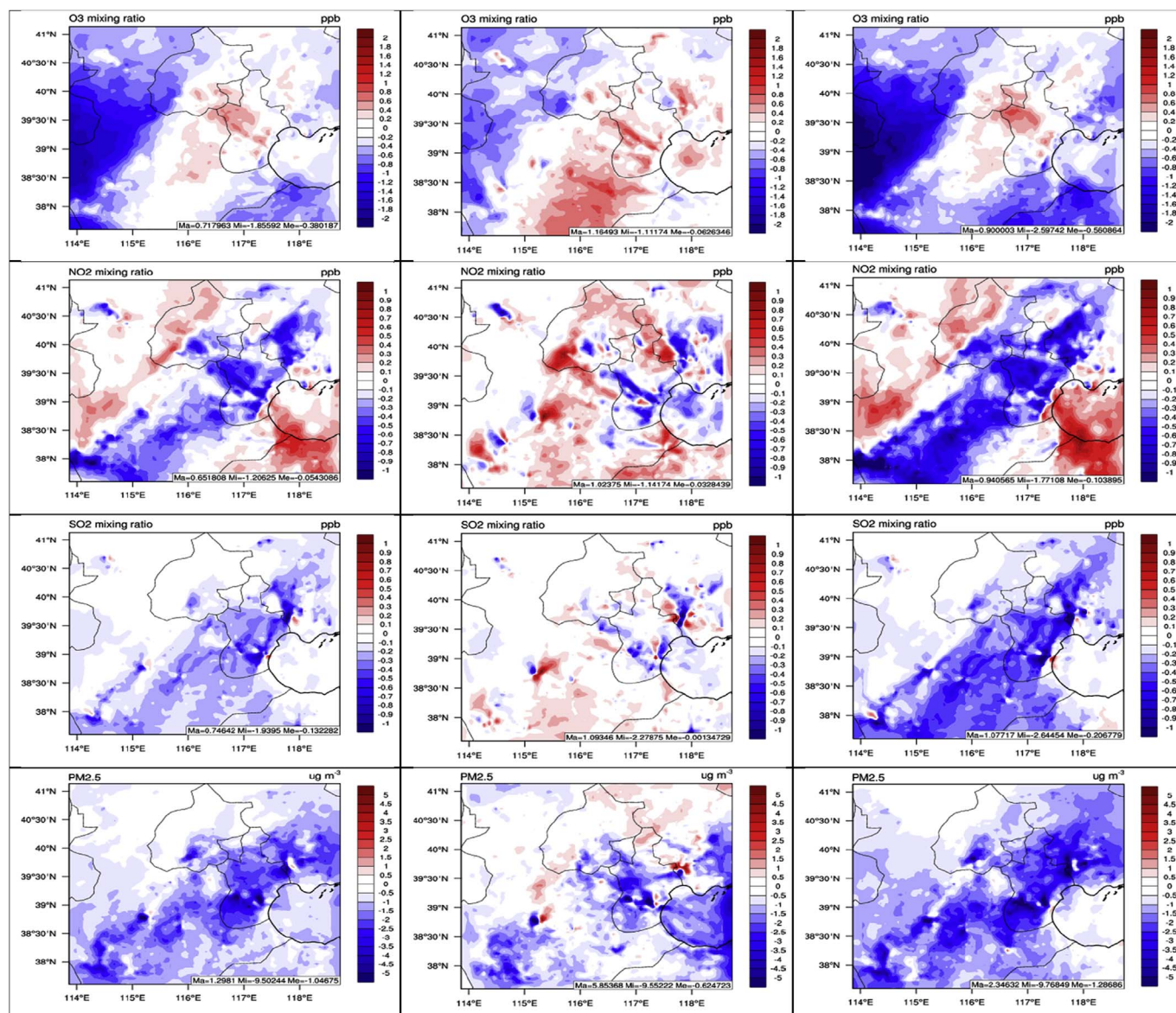
Fig. 12. Differences between SEN1 and SEN2 (FN-FN no dust activation) for O₃, NO₂, SO₂, and PM₂.₅ (from top to bottom) during the whole period (left panel), dust period (center panel), and non-dust period (right panel) in D03 in spring 2010.

chemical variables the fine scale application of the WRF-CAM5 model.

By using the updated FN series aerosol activation scheme, SEN1 shows much larger (potentially excessive) CDNC predictions compared to BASE. The larger predicted CDNC in turn increases LWP, CF, and COT and decreases incoming solar radiation, T2, and precipitation through the aerosol-cloud interactions. The aerosol indirect effects simulated by different aerosol activation treatments can further change the air quality (e.g., decreasing O₃ through reduced radiation and T2 and increasing NO₂ through reduced photolysis rates). The model performance for most of the radiation/cloud variables is further improved by using the FN series scheme. For example, the domain-average NMBs for LWP, CF, and COT have been reduced from −47.5%, −10.6%, and −35.8%, respectively, in BASE to −34.3%, −10.0%, and −24.5%, respectively, in SEN1 at 36-km resolution. The model performance for radiation variables and precipitation has also been slightly improved. The inclusion of adsorptive activation of dust particles (i.e., K09) shows similar impacts on both meteorology and air quality as compared to differences between the FN series and AG schemes, but to a lesser extent. The contribution can be quite significant for some variables (e.g., ~45% contribution from dust for the change of

CDNC in D03) during dust storm episodes compared to the overall differences between the FN and AG schemes.

Compared with a precedent work by Zhang et al. (2015a), although this study uses the same version of model and 36-km outer domain, the emphases are noticeably different. First, this study focuses on a specific episode with extreme dust storm events instead of annual simulations. The dust (surrogated by PM₁₀) performance is comprehensively evaluated and impacts of model biases on aerosol-cloud interactions are investigated. Second, the simulations are conducted over triple-nested domains with a focus on the fine scale resolution. To our knowledge, there are very few fine resolution studies over East Asia (e.g., 4-km) with a focus on aerosol-cloud interactions using advanced online coupled model with aerosol impacts on subgrid cumulus clouds considered. The impacts of fine grid resolutions on model performance are also extensively discussed. Third, impacts of the unique dust adsorptive activation mechanism in the FN series scheme on the cloud formation and regional air quality are more completely examined. It is concluded that the contribution from this mechanism is quite significant during the dust storm events and indicates its importance in modulating regional climate in East Asia.
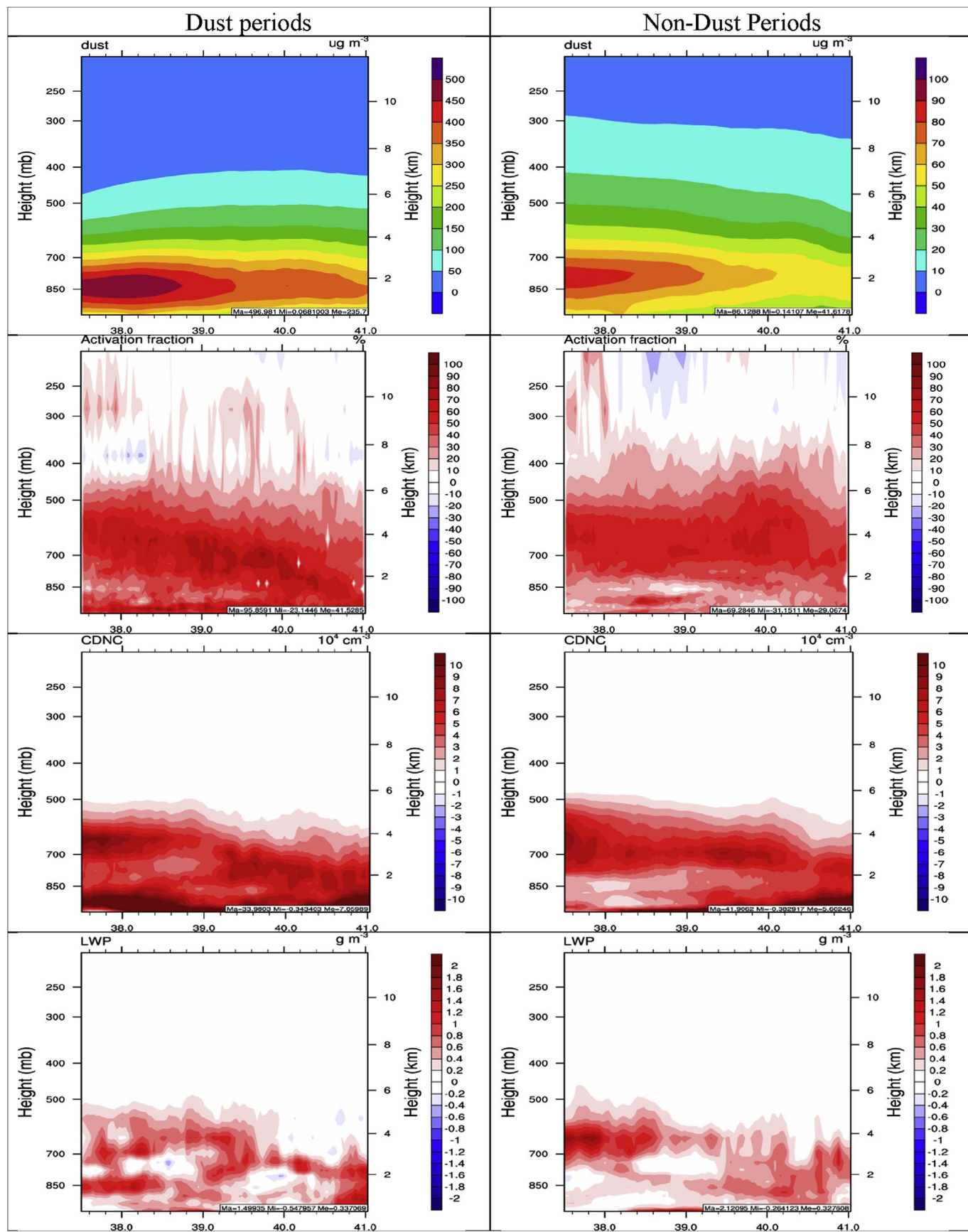
Fig. 13. Zonally-averaged cross-section plots for dust concentrations, differences (SEN1-SEN2) of activation percentage of dust, CDNC, and LWP during dust and non-dust periods in D03 in k spring 2010.

Finally, a few caveats should be noted in this work and may be considered in future model development to further improve the model performance of WRF-CAM5. First, the initial development of the MAM3 aerosol module targeted the study of climate and aerosol-cloud interactions on global scale. To reduce computational cost, nitrate (its contribution to global aerosol loading is relatively low as well) is not treated and only a simplified SOA module is included in MAM3. However for regional climate/air quality studies, the contribution of aerosol nitrate to PM$_{2.5}$ might not be negligible or can even be quite significant during certain episodes (such as winter hazes in East Asia) as reported by previous studies (e.g., Zheng et al., 2015; Zhang et al., 2016). The simplified SOA module has also been found by previous studies (Zhang, 2014; Zhang et al., 2015a) to potentially underestimate the SOA concentrations. Inclusion of aerosol nitrate and more sophisticated SOA treatments will very likely improve the aerosol predictions and potentially improve the aerosol-cloud interactions in WRF-CAM5. Second, as reported by a few studies (e.g., Wang et al., 2012; Zheng et al., 2015), the heterogeneous chemistry on the dust particles during dust storm episodes may significantly increase PM$_{2.5}$ concentrations and also change its composition, which may further affect the aerosol-cloud interactions and should be considered in future model development. Third, it has been noted that the ZM cumulus parameterization has a relatively poor scale sensitivity when applying to resolution finer than 36-km (Yun et al., 2017), which could compromise the model performance at the higher resolutions such as 12- and 4-km.

Acknowledgments

Appendix A. Supplementary data

Supplementary data related to this article can be found at http://dx.doi.org/10.1016/j.atmosenv.2017.12.014.

References

Abdul-Razzak, H., Ghan, S.J., 2000. A parameterization of aerosol activation 2. Multiple aerosol types. J. Geophys. Res. 105 (D5), 6837–6844.

Akimoto, H., 2003. Global air quality and pollution. Science 302, 1716–1719. http://dx.doi.org/10.1126/science.1092666.

Alapaty, K., Herwehe, J.A., Otte, T.L., Nolte, C.G., Bullock, O.R., Mallard, M.S., Kain, J.S., Dudhia, J., 2012. Introducing subgrid-scale cloud feedbacks to radiation for regional meteorological and climate modeling. Geophys. Res. Lett. 39, L24809. http://dx.doi.org/10.1029/2012GL054031.

Andreae, M.O., 2009. Correlation between cloud condensation nuclei concentration and aerosol optical thickness in remote and polluted regions. Atmos. Chem. Phys. 9, 543–556. http://dx.doi.org/10.5194/acp-9-543-2009.

Barahona, D., Nenes, A., 2007. Parameterization of cloud droplet formation in large scale models: including effects of entrainment. J. Geophys. Res. 112, D16206.

Barahona, D., West, R.E.L., Siter, P., Romakkaniemi, S., Kokkola, H., Nenes, A., 2010. Comprehensively accounting for the effect of giant CCN in cloud activation parameterization. Atmos. Chem. Phys. 10, 2467–2473.

Barth, M.C., Rasch, P.J., Kiehl, J.T., Benkovitz, C.M., Schwartz, S.E., 2000. Sulfur chemistry in the national center for atmospheric research community climate model:

description, evaluation, features and sensitivity to aqueous chemistry. J. Geophys. Res. 105, 1387–1415.

Bian, H., Tie, X., Cao, J., Ying, Z., Han, S., Xue, Y., 2011. Analysis of a severe dust storm event over China: application of the WRF-Dust model. Aerosol and Air Quality Research 11, 419–428. http://dx.doi.org/10.4209/aaqr.2011.04.0053.

Boucher, O., Randall, D., Artaxo, P., Bretherton, C., Feingold, G., Forster, P., Kerminen, V.-M., Kondo, Y., Liao, H., Lohmann, U., Rasch, P., Satheesh, S.K., Sherwood, S., Stevens, B., Zhang, X.Y., 2013. Clouds and aerosols. In: Stocker, T.F., Qin, D., Plattner, G.-K., Tignor, M., Allen, S.K., Boschung, J., Nauels, A., Xia, Y., Bex, V., Midgley, P.M. (Eds.), Climate Change 2013: the Physical Science Basis. Contribution of Working Group I to the Fifth Assessment Report of the Intergovernmental Panel on Climate Change. Cambridge University Press, Cambridge, UK and New York, NY, USA.

Bretherton, C.S., Park, S., 2009. A new moist turbulence parameterization in the Community Atmosphere Model. J. Climate 22, 3422–3448.

Chen, F., Dudhia, J., 2001. Coupling an advanced land-surface/hydrology model with the Penn State/NCAR MM5 modeling system. Part I: model implementation and sensitivity. Mon. Wea. Rev. 129, 569–585.

Chen, S., Huang, J., Zhao, C., Qian, Y., Leung, L.R., Yang, B., 2013. Modeling the transport and radiative forcing of Taklimakan dust over the Tibetan Plateau: a case study in the summer of 2006. J. Geophys. Res. Atmos. 118, 797–812. http://dx.doi.org/10.1002/jgrd.50122.

Chen, Y., Zhang, Y., Fan, J., Leung, L.R., Zhang, Q., He, K.-B., 2015. Application of an online-coupled regional climate model, WRF-CAM5, over East Asia for examination of ice nucleation schemes: Part I. Comprehensive model evaluation and trend analysis for 2006 and 2011. Climate 3 (3), 627–667. http://dx.doi.org/10.3390/cli3030627.

Clough, S.A., Shephard, M.W., Mlawer, J.E., Delamere, J.S., Iacono, M.J., Cady-Pereira, K., Boukabara, S., Brown, P.D., 2005. Atmospheric radiative transfer modeling: a summary of the AER codes. J. Quant. Spectrosc. Radiat. Transf. 91 (2), 233–244.

Cohard, J.-M., Pinty, J.-P., Suhre, K., 2000. On the parameterization of activation spectra from cloud condensation nuclei microphysical properties. J. Geophys. Res. 105, 11753–11766. http://dx.doi.org/10.1029/11999JD901195.

Fountoukis, C., Nenes, A., 2005. Continued development of a cloud droplet formation parameterization for global climate models. J. Geophys. Res. 110, D11212.

Fountoukis, C., Koraj, D., van der Gon, H.A.C.D., Charalampidis, P.E., Pilinis, C., Pandis, S.N., 2013. Impact of grid resolution on the predicted fine PM by a regional 3-D chemical transport model. Atmos. Environ. 68, 24–32.

Gantt, B., He, J., Zhang, X., Zhang, Y., Nenes, A., 2014. Incorporation of advanced aerosol activation treatments into CESM/CAM5: model evaluation and impacts on aerosol indirect forcing. Atmos. Chem. Phys. 14, 7485–7497.

García-Díez, M., Fernández, J., Fita, L., Yagüe, C., 2013. Seasonal dependence of WRF model biases and sensitivity to PBL schemes over Europe. Q. J. R. Meteorol. Soc. 139, 501–514. http://dx.doi.org/10.1002/qj.1976.

Ghan, S.J., Abdul-Razzak, H., Nenes, A., Ming, Y., Liu, X., Ovchinnikov, M., Shipway, B., Meskhidze, N., Xu, J., Shi, X., 2011. Droplet nucleation: physically based parameterizations and comparative evaluation. J. Adv. Model. Earth Syst. 3, M10001.

Ghan, S.J., Liu, X., Easter, R.C., Zaveri, R., Rasch, P.J., Yoon, J.-H., Eaton, B., 2012. Toward a minimal representation of aerosols in climate models: comparative decomposition of aerosol direct, semidirect, and indirect radiative forcing. J. Climate 25, 6461–6476.

Gong, S.L., Barrie, L.A., Lazare, M., 2002. Canadian Aerosol Module (CAM): a size-segregated simulation of atmospheric aerosol processes for climate and air quality models: 2. Global sea-salt aerosol and its budgets. J. Geophys. Res. 107 (D24), 4779.

Grell, G.A., Peckham, S.E., Schmitz, R., McKeen, S.A., Frost, G., Skamarock, W.C., Eder, B., 2005. Fully coupled "online" chemistry within the WRF model. Atmos. Environ. 39 (37), 6957–6975. http://dx.doi.org/10.1016/j.atmosenv.2005.04.027.

Guenther, A.B., Karl, T., Harley, P., Wiedinmyer, C., Palmer, P.I., Geron, C., 2006. Estimates of global terrestrial isoprene emissions using MEGAN (model of emissions of Gases and aerosols from nature). Atmos. Chem. Phys. 6, 3181–3210.

Han, X., Ge, C., Tao, J., Zhang, M., Zhang, R., 2012. Air quality modeling for a strong dust event in East Asia in March 2010. Aerosol and Air Quality Research 12, 615–628. http://dx.doi.org/10.4209/aaqr.2011.11.0191.

Heald, C.L., Jacob, D.J., Park, R.J., Alexander, B., Fairlie, T.D., Yantosca, R.M., Chu, D.A., 2006. Transpacific transport of Asian anthropogenic aerosols and its impact on surface air quality in the United States. J. Geophys. Res. 111, D14310. http://dx.doi.org/10.1029/2005JD006847.

Jiménez, P.A., Dudhia, J., González-Rouco, J.F., Montávez, J.P., García-Bustamante, E., Navarro, J., Vilà-Guerau de Arellano, J., Muñoz-Roldán, A., 2013. An evaluation of WRF's ability to reproduce the surface wind over complex terrain based on typical circulation patterns. J. Geophys. Res. 118, 7651–7669. http://dx.doi.org/10.1002/jgrd.50585.

Karydis, V.A., Kumar, P., Barahona, D., Sokolik, I.N., Nenes, A., 2011. On the effect of dust particles on global cloud condensation nuclei and cloud droplet number. J. Geophys. Res. 116, D23204. http://dx.doi.org/10.1029/2011JD016283.

Köhler, H., 1936. The nucleus in the growth of hygroscopic droplets. Trans. Faraday Soc. 32, 1152–1161.

Kuik, F., Lauer, A., Churkina, G., Denier van der Gon, H.A.C.D., Fenner, D., Mar, K.A., Butler, T.M., 2016. Air quality modelling in the Berlin–Brandenburg region using WRF-Chem v3.7.1: sensitivity to resolution of model grid and input data. Geosci. Model Dev. 9, 4339–4363. http://dx.doi.org/10.5194/gmd-9-4339-2016.

Kumar, P., Sokolik, I.N., Nenes, A., 2009. Parameterization of cloud droplet formation for global and regional models: including adsorption activation from insoluble CCN. Atmos. Chem. Phys. 9, 2517–2532.

Li, J., Han, Z., Zhang, R., 2011. Model study of atmospheric particulates during dust storm period in March 2010 over East Asia. Atmos. Environ. 45, 3954–3964. http://dx.doi.org/10.1016/j.atmosenv.2011.04.068.

Lim, K.-S., Fan, J., Leung, L.R., Ma, P.-L., Singh, B., Zhao, C., Zhang, Y., Zhang, G., Song, X., 2014. Investigation of aerosol indirect effects using a cumulus microphysics parameterization in a regional climate model. J. Geophys. Res. 119, 906–926. http://dx.doi.org/10.1002/2013JD020958.

Liu, et al., 2012. Toward a minimal representation of aerosols in climate models: description and evaluation in the Community Atmosphere Model CAM5. Geosci. Model Dev. 5, 709–739.

Ma, P.-L., Rasch, P.J., Fast, J.D., Easter, R.C., Gustafson Jr., W.I., Liu, X., Ghan, S.J., Singh, B., 2013. Assessing the CAM5 physics suite in the WRF-Chem model: implementation, evaluation, and resolution sensitivity. Geosci. Model Dev. 7, 755–778.

Mass, C., Ovens, D., 2010. WRF Model Physics: Progress, Problems, and Perhaps Some Solutions, the 11th WRF Users' Workshop, 21–25 June. Boulder, CO.

McMillen, J.D., Steenburgh, W.J., 2015. Impact of microphysics parameterizations on simulations of the 27 October 2010 Great Salt Lake–effect snowstorm. Weather Forecast. 30, 136–152.

Ming, Y., Ramaswamy, V., Donner, L.J., Phillips, V.T.J., 2006. A new parameterization of cloud droplet activation applicable to general circulation models. J. Atmos. Sci. 63 (4), 1348–1356. http://dx.doi.org/10.1175/JAS3686.1.

Morrison, H., Gettelman, A., 2008. A new two-moment bulk stratiform cloud microphysics scheme in the Community Atmosphere Model, Version 3 (CAM3). Part I: description and numerical tests. J. Climate 21, 3642–3659.

Nenes, A., Seinfeld, J.H., 2003. Parameterization of cloud droplet formation in global climate models. J. Geophys. Res. 108 (D14), 4415.

Niemand, M., Mohler, O., Vogel, B., Vogel, H., Hoose, C., Connolly, P., Klein, H., Bingemer, H., DeMott, P., Skrotzki, J., Leisner, T., 2012. A particle-surface-area-based parameterization of immersion freezing on desert dust particles. J. Atmos. Sci. 69, 3077–3092.

Park, S.-U., Choe, A., Park, M.-S., 2012. A simulation of Asian dust events in March 2010 by using the ADAM2 model. Theor. Appl. Climatol. 107 (3), 491–503.

Pei, L., Moore, N., Zhong, S., Luo, L., Hyndman, D.W., Heilman, W.E., Gao, Z., 2014. WRF model sensitivity to land surface model and cumulus parameterization under short-term climate extremes over the southern great plains of the United States. J. Climate 27, 7703–7724.

Queen, A., Zhang, Y., 2008. Examining the sensitivity of MM5-CMAQ predictions to explicit microphysics schemes and horizontal grid resolutions, Part III - the impact of horizontal grid resolution. Atmos. Environ. 42, 3869–3881.

Song, X., Zhang, G.J., 2011. Microphysics parameterization for convective clouds in a global climate model: description and single-column model tests. J. Geophys. Res. 116, D02201.

Tie, X., Madronich, S., Walters, S., Zhang, R., Racsh, P., Collins, W., 2003. Effect of clouds on photolysis and oxidants in the troposphere. J. Geophys. Res. 108 (D20), 4642.

Tuccella, P., Curci, G., Visconti, G., Bessagnet, B., Menut, L., Park, R.J., 2012. Modeling of gas and aerosol with WRF/Chem over Europe: evaluation and sensitivity study. J. Geophys. Res. 117, D03303. http://dx.doi.org/10.1029/2011JD016302.

US EPA, 2007. Guidance on the Use of Models and Other Analyses for Demonstrating Attainment of Air Quality Goals for Ozone, $PM_{2.5}$ and Regional Haze. The U.S. Environmental Protection Agency, Research Triangle Park EPA-454/B-07–002.

Wang, K., Zhang, Y., Jang, C., Phillips, S., Wang, B., 2009. Modeling intercontinental air pollution transport over the trans-Pacific region in 2001 using the Community Multiscale Air Quality modeling system. J. Geophys. Res. 114, D04307. http://dx.doi.org/10.1029/2008JD010807.

Wang, K., Zhang, Y., Nenes, A., Fountoukis, C., 2012. Implementation of dust emission and chemistry into the Community Multiscale Air Quality Modeling System and initial application to an Asian dust storm episode. Atmos. Chem. Phys. 12, 10209–10237. http://dx.doi.org/10.5194/acp-12-10209-2012.

Wang, L., Jang, C., Zhang, Y., Wang, K., Zhang, Q., Streets, D., Fu, J., Lei, Y., Schreifels, J., He, K., Hao, J., Lam, Y.-F., Lin, J., Meskhidze, N., Voorhees, S., Evarts, D., Phillips, S., 2010. Assessment of air quality benefits from national air pollution control policies in China. Part I: background, emission scenarios and evaluation of meteorological predictions. Atmos. Environ. 44, 3442–3448. http://dx.doi.org/10.1016/j.atmosenv.2010.05.051.

Yu, S., 2000. The role of organic acids (formic, acetic, pyruvic and oxalic) in the formation of cloud condensation nuclei (CCN): a review. Atmos. Res. 53, 185–217.

Yu, S., Mathur, R., Pleim, J., Wong, D., Gilliam, R., Alapaty, K., Zhao, C., Liu, X., 2014. Aerosol indirect effect on the grid-scale clouds in the two-way coupled WRF-CMAQ:

model description, development, evaluation and regional analysis. Atmos. Chem. Phys. 14, 11247–11285. http://dx.doi.org/10.5194/acp-14-1-2014.

Yun, Y., Fan, J., Xiao, H., Zhang, G.J., Ghan, S.J., Xu, K.-M., Ma, P.-L., Gustafson, W.I., 2017. Assessing the resolution adaptability of the Zhang-Mcfarlane cumulus parameterization with spatial and temporal averaging. J. Adv. Model. Earth Syst. 9. https://doi.org/10.1002/2017MS001035.

Zaveri, R.A., Peters, L.K., 1999. A new lumped structure photochemical mechanism for large-scale applications. J. Geophys. Res. 104 (D23), 30387–30415. http://dx.doi.org/10.1029/1999JD900876.

Zender, C.S., Bian, H., Newman, D., 2003. Mineral dust entrainment and deposition (DEAD) model: description and 1990s dust climatology. J. Geophys. Res. 108, 4416. http://dx.doi.org/10.1029/2002JD002775.

Zhang, G.J., McFarlane, N.A., 1995. Sensitivity of climate simulations to the parameterization of cumulus convection in the Canadian Climate Centre general circulation model. Atmos.-Ocean 33, 407–446.

Zhang, Q., et al., 2009. Asian emissions in 2006 for the NASA INTEX-B mission. Atmos. Chem. Phys. 9, 5131–5153. http://dx.doi.org/10.5194/acp-9-5131-2009.

Zhang, X., 2014. Examining Aerosol Indirect Effects Using a Regional Climate-aerosol Model with Improved Aerosol Activation and Cloud Parameterizations. Master thesis, 196 pp. North Carolina State University, Raleigh.

Zhang, X.Y., Gong, S.L., Shen, Z.X., Mei, F.M., Xi, X.X., Liu, L.C., Zhou, Z.J., Wang, D., Wang, Y.Q., Cheng, Y., 2003. Characterization of soil dust aerosol in China and its transport and distribution during 2001 ACE-Asia: 1. Network observations. J. Geophys. Res. 108, 4261. http://dx.doi.org/10.1029/2002JD002632. D9.

Zhang, Y., Liu, P., Pun, B., Seigneur, C., 2006. A comprehensive performance evaluation of MM5-CMAQ for summer 1999 Southern Oxidants Study episode, Part-I. Evaluation protocols, databases and meteorological predictions. Atmos. Environ. 40, 4825–4838.

Zhang, Y., Wen, X.-Y., Jang, C.J., 2010. Simulating chemistry-aerosol-cloud-radiation-climate feedbacks over the continental U.S. using the online-coupled Weather Research Forecasting Model with chemistry (WRF/Chem). Atmos. Environ. 44, 3568–3582.

Zhang, Y., Cheng, S.-H., Chen, Y.-S., Wang, W.-X., 2011. Application of MM5 in China: model evaluation, seasonal variations, and sensitivity to horizontal grid resolutions. Atmos. Environ. 45, 3454–3465.

Zhang, Y., Chen, Y.-C., Sarwar, G., Schere, K., 2012a. Impact of gas-phase mechanisms on WRF/Chem predictions: mechanism implementation and comparative evaluation. J. Geophys. Res. 117, D01301. http://dx.doi.org/10.1029/2011JD015775.

Zhang, Y., Karamchandani, P., Glotfelty, T., Streets, D.G., Grell, G., Nenes, A., Yu, F.-Q., Bennartz, R., 2012b. Development and initial application of the global-through-urban weather research and forecasting model with chemistry (GU-WRF/Chem). J. Geophys. Res. 117, D20206. http://dx.doi.org/10.1029/2012JD017966.

Zhang, Y., Sartelet, K., Zhu, S., Wang, W., Wu, S.-Y., Zhang, X., Wang, K., Tran, P., Seigneur, C., Wang, Z.-F., 2013. Application of WRF/Chem-MADRID and WRF/Polyphemus in Europe - Part 2: evaluation of chemical concentrations and sensitivity simulations. Atmos. Chem. Phys. 13, 6845–6875. http://dx.doi.org/10.5194/acp-13-6845-2013.

Zhang, Y., Zhang, X., Wang, K., He, J., Leung, L.R., Fan, J.-W., Nenes, A., 2015a. Incorporating an advanced aerosol activation parameterization into WRF-CAM5: model evaluation and parameterization intercomparison. J. Geophys. Res. 120, 6952–6979. http://dx.doi.org/10.1002/2014JD023051.

Zhang, Y., Chen, Y., Fan, J., Leung, L.R., 2015b. Application of an online-coupled regional climate model, WRF-CAM5, over East Asia for examination of ice nucleation schemes: Part II. Sensitivity to ice nucleation parameterizations and dust emissions. Climate 3 (3), 753–774. http://dx.doi.org/10.3390/cli3030753.

Zhang, Y., Zhang, X., Wang, K., Zhang, Q., Duan, F., He, K., 2016. Application of WRF/Chem over East Asia: Part II. Model improvement and sensitivity simulations. Atmos. Environ. 124, 301–320. http://dx.doi.org/10.1016/j.atmosenv.2015.07.023.

Zhao, J., Zhang, F., Xu, Y., Chen, J., Yin, L., Shang, X., Xu, L., 2011. Chemical characteristics of particulate matter during a heavy dust episode in a coastal city, Xiamen, 2010. Aerosol and Air Quality Research 11, 299–308.

Zheng, B., Zhang, Q., Zhang, Y., He, K.B., Wang, K., Zheng, G.J., Duan, F.K., Ma, Y.L., Kimoto, T., 2015. Heterogeneous chemistry: a mechanism missing in current models to explain secondary inorganic aerosol formation during the January 2013 haze episode in North China. Atmos. Chem. Phys. 15, 2031–2049. http://dx.doi.org/10.5194/acp-15-2031-2015.